From Department of Molecular Medicine and Surgery
Karolinska Institutet, Stockholm, Sweden

DIAGNOSTIC PRECISION AND SEX DIFFERENCES IN QUANTITATIVE CARDIOVASCULAR MAGNETIC RESONANCE

Jannike Nickander

Stockholm 2018

Cover:

Different images acquired with cardiovascular magnetic resonance. Top row from left to right: native T1 map, extracellular volume map, and a late gadolinium enhancement image. Second row from the left to right: synthetic late gadolinium enhancement image, myocardial blood volume map, extracellular volume map, myocardial blood volume map during adenosine stress and a myocardial perfusion map, also during adenosine stress. The image in the middle is a native T2 map.

Back cover image by Fredrik Nickander

Diagnostic precision and sex differences in quantitative cardiovascular magnetic resonance

THESIS FOR DOCTORAL DEGREE (Ph.D.)

By

Jannike Nickander, MD

Principal Supervisor:
Martin Ugander, MD, PhD, Associate Professor
Karolinska Institutet
Department of Molecular Medicine and Surgery
Unit of Clinical Physiology

Co-supervisor(s):
Peder Sörensson, MD, PhD
Karolinska Institutet
Department of Molecular Medicine and Surgery
Unit of Clinical Physiology

Andreas Sigfridsson, PhD
Karolinska Institutet
Department of Molecular Medicine and Surgery
Unit of Clinical Physiology

Kenneth Caidahl, MD, PhD, Professor
Karolinska Institutet
Department of Molecular Medicine and Surgery
Unit of Clinical Physiology

Opponent:
Chiara Bucciarelli-Ducci, MD, PhD, FESC, FRCP
University of Bristol
Bristol Medical School
Translation Health Sciences

Examination Board:
Karin Schenck-Gustafsson, MD, PhD, Professor
Karolinska Institutet
Department of Medicine
Unit of Cardiology

Birgitta Janerot, MD, PhD, Professor
Karolinska Institutet
Department of Clinical Sciences,
Intervention and Technology
Unit of Functional Imaging and Technology

Erik Hedström, MD, PhD, Associate Professor
Lund University
Department of Clinical Sciences Lund
Unit of Clinical Physiology and Diagnostic
Radiology

"If we knew what it was we were doing it would not be called research, would it?"

Albert Einstein

ABSTRACT

Correct medical treatment necessitates a correct diagnosis. Cardiac imaging aims to establish an accurate diagnosis without performing unnecessary invasive procedures. Cardiovascular magnetic resonance (CMR) has emerged as a valuable diagnostic tool in clinical cardiology because of its inherently good soft-tissue contrast, dynamic visualizations and the possibility to perform quantitative tissue characterization. However, diagnostic precision may be affected in quantitative imaging by several factors such as the presence of sex differences, or measurements errors. Therefore, the aim of this thesis was to identify parameters and sex differences that affect precision and accuracy, and to evaluate post-processing methods to increase diagnostic precision.

We found that intramyocardial blood affects native myocardial T_1 values in patients without focal abnormalities, and that native myocardial T_1 values differ between the sexes. We developed a blood correction model that maintained an increase in diagnostic precision by 13% when applied to an independent patient cohort, which furthermore also eliminated sex differences in healthy volunteers in Study I. In Study II, we evaluated a post-processing method called stationary tissue background correction for increasing diagnostic precision in clinical blood flow measurements. We found that the number of patients with a pulmonary-to-systemic blood flow ratio (Qp/Qs) outside of the normal range decreased following stationary tissue background correction. In Study III, we investigated the presence of sex differences in a newly developed myocardial perfusion imaging sequence in healthy volunteers. We found that women have higher myocardial blood volume, myocardial perfusion and myocardial extracellular volume compared to men both at rest and during adenosine stress, which provide mechanistic insight into myocardial physiology. In Study IV, we investigated the clinical accuracy and precision of synthetic scar images (SynLGE) from post-contrast T_1 maps compared to conventional scar images (LGE) for diagnosing focal myocardial fibrosis of any etiology. Compared to LGE, SynLGE yielded a sensitivity of 77%, a specificity of 98%, a positive predictive value of 97% and a negative predictive value of 86%.

In conclusion, there are sex differences in several aspects of clinical quantitative CMR imaging that may affect diagnostic precision. Post-processing is a powerful tool to improve diagnostic precision both by increasing precision in native myocardial T_1 values via blood correction, and in Qp/Qs via stationary tissue background correction. SynLGE can provide complementary confidence in the assessment of focal myocardial fibrosis in complement to conventional LGE, and thereby increase diagnostic accuracy and precision.

LIST OF SCIENTIFIC PAPERS

I. **Nickander J**, Lundin M, Abdula G, Sorensson P, Rosmini S, Moon JC, Kellman P, Sigfridsson A, and Ugander M. Blood correction reduces variability and gender differences in native myocardial T1 values at 1.5 T cardiovascular magnetic resonance - a derivation/validation approach. *J Cardiovasc Magn Reson*. 2017;19(1):41

II. **Nickander J**, Lundin M, Abdula G, Jenner J, Maret E, Sorensson P, Heiberg E, Sigfridsson A, Ugander M. Stationary tissue background correction improves precision of the pulmonary-to-systemic blood flow ratio by phase contrast velocity encoded cardiovascular magnetic resonance. *Submitted*

III. **Nickander J**, Themudo R, Sigfridsson A, Xue H, Kellman P and Ugander M. Females have higher myocardial blood volume, myocardial perfusion and myocardial extracellular volume compared to males – both at rest and during adenosine stress cardiovascular magnetic resonance. *Submitted*

IV. Abdula G, **Nickander J**, Sorensson P, Lundin M, Kellman P, Sigfridsson A and Ugander M. Synthetic late gadolinium enhancement cardiac magnetic resonance for diagnosing myocardial scar. *Scand Cardiovas J*, 2018, *In press. DOI:10.1080/14017431.2018.1449960.*

CONTENTS

LIST OF ABBREVIATIONS

ACS	Acute coronary syndrome
AIF	Arterial input function
AMI	Acute myocardial infraction
bSSFP	balanced steady state free precession
CAC	Coronary calcium score
CT	Computed tomography
CCTA	Coronary computed tomography angiography
CCU	Coronary care unit
CFR	Coronary flow reserve
CMR	Cardiovascular magnetic resonance
CSF	Coronary sinus flow
CVD	Cardiovascular disease
ECG	Electrocardiogram
ECV	Extracellular volume
FA	Flip angle
FFR	Fractional flow reserve
FLASH	Fast low angle shot
INOCA	Ischemia with non-obstructive coronary arteries
IR	Inversion recovery
LGE	Late gadolinium enhancement
LV	Left ventricular
MBF	Myocardial blood flow
MBV	Myocardial blood volume
MCE	Myocardial contrast echocardiography
MINCA	Myocardial infarction with normal coronary arteries
MINOCA	Myocardial infraction with non-obstructive coronary arteries
MOLLI	Modified Look-Locker inversion recovery
MPI	Myocardial perfusion imaging
MRI	Magnetic resonance imaging
NM	Nuclear medicine imaging

NSF	Nephrogenic systemic fibrosis
Non STEMI	Non ST elevation myocardial infarction
NPV	Negative predictive value
PET	Positron emission tomography
PPV	Positive predictive values
PSIR	Phase sensitive inversion recovery
Qp/Qs	Pulmonary to systemic blood flow ratio
RBC	Red blood cells
RF	Radio frequency
RFR	Relative CFR
ROI	Region of interest
RPP	Rate pressure product
SAPPHIRE	Saturation pulse prepared heart rate independent inversion recovery
SASHA	Saturation recovery single shot acquisition
ShMOLLI	Short modified Look Locker inversion recovery
SI	Signal intensity
SPECT	Single-photon emission computed tomography
SR	Saturation recovery
SSFP	Steady state free precession
STEMI	ST elevation myocardial infarction
SynLGE	Synthetic late gadolinium enhancement
T	Tesla
TI	Inversion time
TR	Repetition time

1 INTRODUCTION

Correct medical treatment necessitates a correct diagnosis. Cardiac imaging aims to establish an accurate diagnosis without performing unnecessary invasive procedures. Several non-invasive cardiac imaging modalities are in clinical use today. Echocardiography, cardiac computed tomography (CT), cardiac nuclear medicine imaging (NM), and CMR all convey valuable diagnostic information about the heart's anatomy and function. However, each technique has limitations ranging from radiation burden to the inability to perform myocardial tissue characterization.

Echocardiography generates images from ultrasound waves that are reflected in the heart and detected by a transducer. Echocardiography is particularly suitable for assessing the motion of the left ventricular (LV) wall, as well as identifying functional abnormalities [1], valve abnormalities and pericardial effusion. While echocardiography is readily available, this imaging method has a limited ability to directly characterize myocardial tissue properties [2]. Cardiac CT has evolved into an important imaging method to evaluate coronary calcification [2], cardiac and coronary anatomy, and function [3]. The established method to quantify coronary calcification, the coronary artery calcium (CAC) score, can predict the likelihood of coronary events [4]. Coronary CT angiography (CCTA) is another important cardiac CT technique. CCTA has a very high specificity and negative predictive value (NPV). Therefore, CCTA is an appropriate tool to use for intermediate risk patients who present with chest pain in the emergency room, to rule out acute coronary syndrome (ACS) [5, 6]. NM is an important tool for myocardial perfusion imaging (MPI) and viability assessment with the use of radiotracers in positron emission tomography (PET) and single-photon emission computed tomography (SPECT) [7]. PET enables non-invasive absolute quantification of myocardial perfusion, which is also sometimes referred to myocardial blood flow (MBF). By calculating the ratio of the peak perfusion at maximal pharmacological vasodilation to perfusion at rest, the coronary flow reserve (CFR) can be calculated. CFR is an important measure for evaluating the functional relevance of a coronary stenosis [8, 9]. Prior to the year 2000, PET was regarded as the reference standard for myocardial viability imaging. However, since the introduction of the CMR technique known as late gadolinium enhancement (LGE), which allows for detailed tissue characterization, LGE CMR has become the modality of choice for viability imaging [10].
CMR has emerged as a robust imaging technique for a comprehensive set of states including cardiac anatomical morphology [11], tissue characterization [12-15], LV and right ventricular function [2, 16], myocardial wall thickness and viability [10, 17], myocardial perfusion [18-20], and blood flow [21]. Consequently, CMR has become an important diagnostic and scientific tool in clinical cardiology.

Why is it important to know the correct diagnosis? Cardiovascular disease (CVD) is the leading cause of death [22] globally. Many lives can be saved, and quality of life improved if we correctly can identify patients that are in need of treatment. This thesis aims to evaluate the diagnostic precision of several clinical CMR methods, identify areas of improvement, and

even in some cases propose new improved methods to increase diagnostic accuracy and precision of CMR.

1.1 IMPORTANT CONCEPTS

Before elaborating on the background of clinical CMR and its role in clinical diagnostics, there are a few important concepts that need to be defined.

1.1.1 Sex and gender

Sex and gender are two different concepts that often interact in disease. However, they have separate, distinct definitions according to the Canadian Institutes of Health Research [23]. Sex include the biological characteristics of both humans and animals, and biological attributes include both physical and physiological features. These features comprise of chromosomes, and gene expression, but also hormone levels and function, as well as reproductive anatomy. Gender, on the other hand, refers to the social construction of roles, expressions, behaviors and personalities of individual boys, men, girls, women and gender diverse, non-binary individuals. Gender is closely linked to how people perceive each other and themselves, and influences how people act and interact. Gender is often described as binary (woman and man). However, gender is experienced and expressed with a great variety in different individuals and groups. It is important to separate these concepts as the physiological factors and the social constructions affect CVD differently.

1.1.2 Accuracy and precision

There are two concepts that can be used to described how we know what we think we know when discussing any diagnostic measurement. These two concepts are **accuracy** and **precision** (Figure 1.1). Accuracy and precision help to describe the diagnostic measurement in terms of how *variable* the test results are, and *how close to the true value* the test results are [24]. Precision describes the random errors that occur when measuring a quantity, it is a measure of statistical variability. Accuracy describe the systematic error that occurs when measuring a quantity, it is a measure of statistical bias; the difference between the measured result and the true value of the quantity.
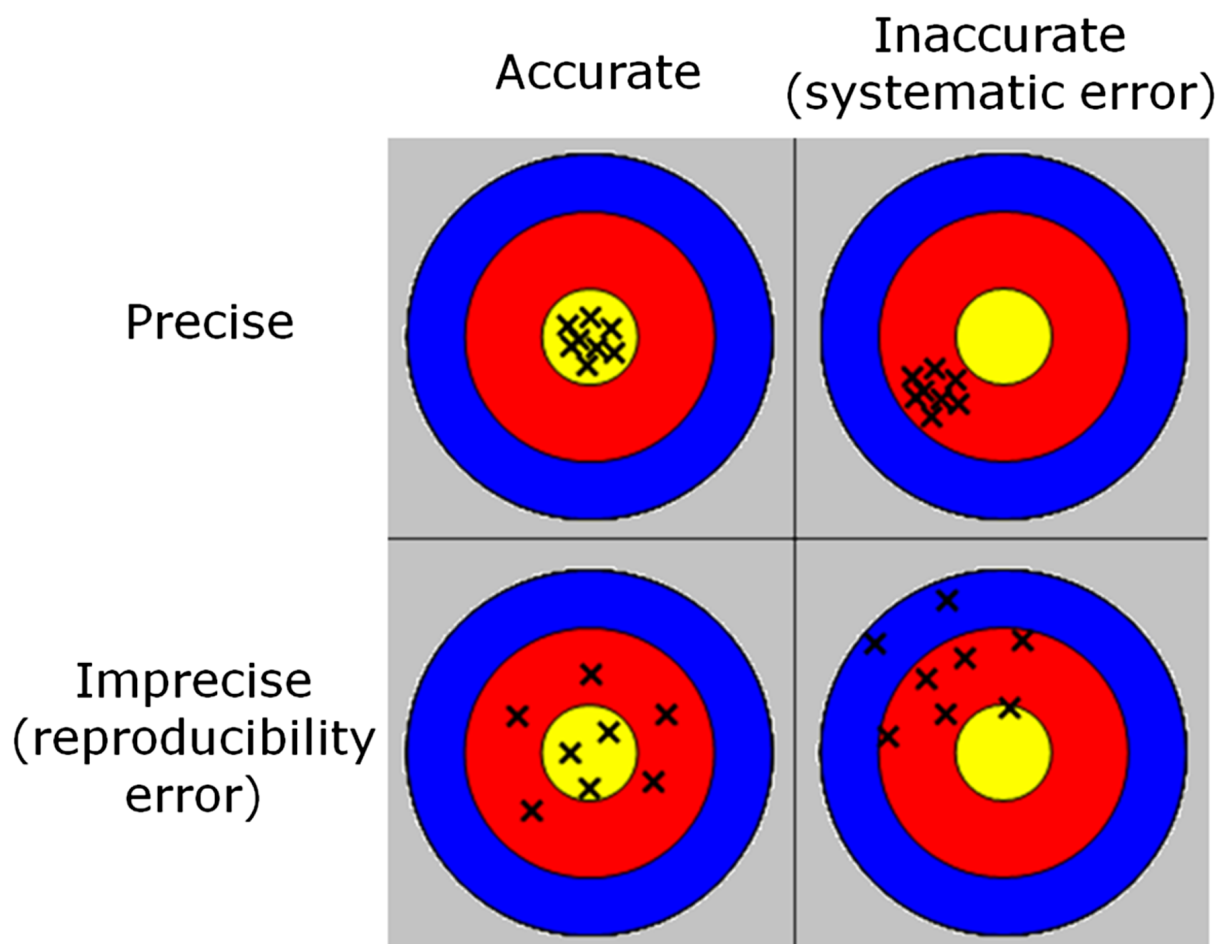
Figure 1.1 Accuracy and precision. *The figure illustrates the two concepts accuracy (columns), and precision (rows), with the bulls-eye representing the true values. The two concepts are completely independent of each other. A diagnostic test can be accurate and precise, as shown in the top left corner where all measurements are within the yellow circle. However, a diagnostic test can be inaccurate, not close to the true value, but yet be precise, meaning that the measurement variability is low. This is illustrated in the top right corner, where all measurements are outside the yellow circle, but the measurements are very close to each other. A diagnostic test can also be accurate, but imprecise, meaning that the measurement variability is high, which is illustrated by the bottom left corner. The measurements are evenly distributed around the yellow circle, close to the true value, however the measurements are far apart, representing the high measurement variability. The bottom right corner shows a diagnostic test that is both inaccurate and imprecise, and the measurements are not close to the yellow circle, and spread apart from each other. Reproduced from[25].*

Given a set of diagnostic measurements, the set can be called precise if the measurements are all close to the average value of the quantity being measured, while the set is accurate if the measurement are close to the true value of the quantity being measured. Accuracy and precision are independent of each other, so a set of diagnostic measurements can be either accurate or precise, or both, or neither [24]. A diagnostic measurement should preferably by both accurate and precise, however there are many measurements in clinical use that are only

accurate or precise, and this will be further exemplified and discussed with T_1 mapping in Section 2.3.

1.1.3 Sensitivity, specificity, predictive values and Bayes theorem

Other approaches to evaluate the performance of a diagnostic test include the terms sensitivity and specificity, as illustrated in Table 1.1. Sensitivity is the percent of true sick people where the test is positive for that disease. Sensitivity answers the question: in case a disease is present, what is the probability of a positive test? Specificity is the percent of healthy people where the test is negative for that disease. Specificity answers the question: in case a disease is absent, what is the probability of a negative test? [26]. For screening, it is essential to have a diagnostic test with high sensitivity, so that the diagnostic test identifies individuals that are truly sick. A test with high specificity can be used to rule out a certain disease, or to be certain that it is time to start a specific treatment.

Predictive values describe the performance of the diagnostic test by indicating the accuracy of the test. The positive predictive value (PPV) reflects the proportion of positive test results that are truly positive, whereas NPV reflects the proportion of negative test results that indeed are negative.

Table 1.1 Representation of sensitivity and specificity.

	Sick (disease present)	Healthy (disease absent)
Positive test	A	B
Negative test	C	D

Sensitivity = A/(A+C), how many of patients (in %) that are sick, are positively identified with the test. Specificity = B/(B+D), how many patients (in %) that are truly healthy, have a negative test. PPV = A/(A+B), how many of the positive test results are truly positive (%). NPV = C/(C+D), how many negative test results are indeed negative (%).

Bayes theorem

Bayes theorem is used to decide the probability of an event, given knowledge of conditions that are related to the event. It enables an *a priori* estimation of the chances of a certain diagnosis to be merged with the eventual test results. This allows for an *a posteriori* assessment of the diagnosis, and in its essence reflecting clinical decision making [26]. Therefore, Bayes theorem is easily applicable to medical diagnostics. The probability of a test being positive for a certain disease is related to the probability of the disease prior to undergoing the diagnostic test (pre-test probability, PTP). If the PTP is low, like in young individuals for ischemic heart disease, testing for ischemic heart disease will therefore not

add diagnostic information. Instead, there is a risk for false positive results, which brings added risk for the patient, i.e. in the form of unnecessary procedures or treatments.

2 CARDIOVASCULAR MAGNETIC RESONANCE

CMR can be performed repeatedly without any known hazardous side effects as the subject is not exposed to ionizing radiation, as in the case with cardiac CT and NM. Side effects can however be caused by the intravenous injection of gadolinium-based CMR contrast agents. Severe allergic reactions are exceedingly rare. The contrast agents may cause nephrogenic systemic fibrosis (NSF), however only in patients with severe renal disease [27]. An incidence of NSF after gadolinium-enhanced CMR was estimated to be 0.0002%-0.039% in 2008 [28]. Recent studies suggest that there is a risk for brain deposition of gadolinium after repeated infusions [29, 30]. There is currently no evidence linking gadolinium deposition in the brain to neurological dysfunction, however the United States National Institutes of Health (NIH) warrants an institutional review of gadolinium administration policies [31]. Another disadvantage of CMR is the relatively long scan time, and the scan may be stressful for the patient, in particular those with claustrophobia. CMR is a relatively expensive imaging modality compared to echocardiography, with a typical cost in Sweden of approximately 10,000 SEK and 3,000 SEK, respectively. However, CMR has become the clinical and scientific method of choice at many centers for characterizing ischemic and non-ischemic heart diseases [12].

2.1 PHYSICS GOVERNING CARDIOVASCULAR MAGNETIC RESONANCE

There are elaborate and complex procedures to generate the actual CMR images that the clinicians use to diagnose patients. This section will briefly describe the basics of Magnetic Resonance Imaging (MRI), in order to provide a basis for the discussion of the different CMR methods used in this thesis. MRI is based on the principle of nuclear magnetic resonance, and can be used to image the intrinsic magnetic properties of tissues. Three main parts constitutes an MRI scanner: the static magnetic field, the radio frequency (RF) coils and gradient coils. The static magnetic field, also called B_0, is generated by a superconductive electromagnet, which is cooled with liquid helium to 4 Kelvin. Typically, the B_0 field of MRI scanners that are used clinically have a magnetic field strength of 1.5 Tesla (T) or 3 T. However, in laboratory settings up to 21 T have been used for imaging animals. Gradient and RF coils will be discussed further in the following sections.

2.1.1 Spins – basis for signal generation

MRI can produce detailed images of complex anatomical structures by imaging the intrinsic properties of tissues. How is this possible?

Spin is a quantum property of elementary particles. The protons and neutrons in the atomic nucleus possess spin. In nuclei with an even number of protons and/or neutrons, the spins cancel out, but if the number is odd the nucleus possesses a net spin [32], which is the basis for the signal produced in MRI. Any species of nuclei with a net spin can be used, but the hydrogen atom is most commonly used for clinical imaging, due to its abundance in the human body as we are mostly made of water. The hydrogen nucleus consists of a single

proton, which, when placed in an external magnetic field, induces a local magnetic field as it spins around its own axis, making it behave similarly to a small bar magnet. The spins (spin vectors) of the hydrogen atoms in a sample (i.e. any given tissue) are randomly oriented until they are subjected to an external magnetic field, which causes the spins (vectors) to align along the direction of that magnetic field [33]. Spin, being a quantum mechanical concept, can only exist in quantized states. This is often described as protons aligning in a spin-up or a spin-down state, where the distribution between the states generates a net magnetization vector. This happens inside the body when a patient enters the scanner, the spins align with B_0 and the resulting net magnetization vector of the tissue (also called magnetization) can be used to generate an image signal.

2.1.2 Generating the signal

By applying a second, time-varying, magnetic field (B_1) for a brief period of time, the net magnetization vector will turn at an angle from B_0. The application of B_1 causes the spins to precess around B_1, the new magnetic field. If B_1 is applied along the y-axis, this will cause the magnetization to flip towards the x-axis. B_1 has to be transmitted at a precession frequency specific to the hydrogen nucleus, which depends on the local field strength. This is because the rate of precession is governed by the magnetic field that causes the precession, according to Equation 1.1

$$\omega = \gamma * B_0$$

where the proportionality constant, γ, is the gyromagnetic ratio and ω is called the Larmor frequency [34]. As the Larmor frequency at the field strengths used for clinical MRI scanning falls within the RF spectrum, the second magnetic field (B_1) applied to move the net magnetization away from B_0, is called an RF pulse and is applied by RF coils.

Before going into magnetization relaxation and the use of gradient coils, we need some common ground or reference to further discuss the spatial movements of the magnetization. The direction of B_0, denoted z, is positioned along the tube of the MR scanner. Since precession about B_0 is always present, it is common to define the coordinate system such that the xy-plane rotates about the z axis (Figure 2.1). Another important concept is phase. The magnetization vector has two basics properties, magnitude and direction. When a signal is measured, is it measured in the xy-plane, and the angle of magnetization in this plane will affect the signal and is known as phase. The ensemble of spins can be described as being in phase, rendering a higher signal amplitude, or out of phase, rendering a lower signal amplitude.
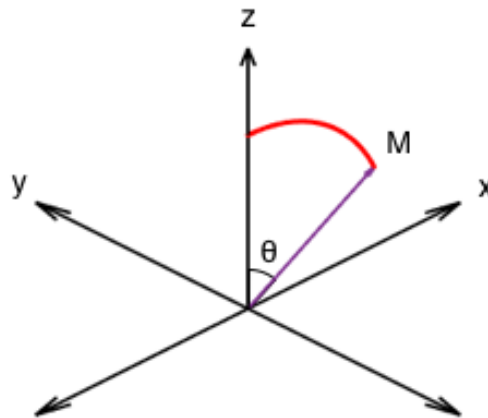
Figure 2.1. Schematic visualization of the spatial movements of the magnetization. *This diagram shows a rotating frame of reference. This means that the xy-plane is rotating about the z-axis with the same angular frequency as the magnetization vector, i.e. the Larmor frequency. A rotating frame of reference allows for a simplified visualization of the spatial movements of the magnetization. In this case, a radio frequency pulse has been applied to move the magnetization away from B_0 at an angle θ.*

2.1.2.1 The intrinsic properties of tissues – T_1 and T_2

The net magnetization vector, induced by B_0 along the z-axis, will flip by a given angle towards the x-axis, when an RF pulse is applied along the y-axis. The given angle will be determined by the RF pulse, depending on the magnitude and duration of that RF pulse. The net magnetization vector has two different magnetization components – the transverse component (within the xy-plane) and the longitudinal component (along the z-axis). By applying an RF pulse of 90°, the entire longitudinal magnetization is now in the transverse plane. If the RF pulse purpose is to convert equilibrium magnetization into transversal magnetization, it is commonly known as an excitation pulse. The resultant transverse magnetization can now be measured by receiver coils. Immediately following the RF pulse, the spins precess in coherence, which induces a current in the receiver coils. But what happens over time following the RF pulse excitation? When the RF pulse is turned off, the net magnetization vector begins to return to the equilibrium position aligned in the B_0 direction, which is along the z-axis, where the spins experience the lowest energy state. Two things happen simultaneously, the magnetization in the xy-plane starts to decay (the transverse component), and the magnetization along the z-axis starts to recover (the longitudinal component). The magnetization decay is caused by so called spin-spin interactions, where the spins interact with each other, and also by small inhomogeneities in the magnetic field [33]. Both of these factors affect the rate and phase of precession, and thereby decreasing coherence of the spins, which leads to a decrease in the signal. Spin-spin

interactions reflect the composition of the tissue, whereas the magnetic field inhomogeneities can both reflect the environment of the tissue, such as presence of iron, but also the hardware of the scanner. The magnetization decay due to spin-spin interactions is called T2 relaxation, whereas the combined decay (spin-spin interaction and field inhomogeneities) is called T2* relaxation. T2* and T2 relaxation is described by Equation 1.2, and Equation 1.3.

$$M_y = M_0 * e^{\frac{-t}{T_2*}}$$

$$\frac{1}{T_2*} = \frac{1}{T_2} + \gamma\Delta B_0$$

where M_y is the magnetization along the y-axis, M_0 is the initial magnetization, t is the time after the RF pulse, and $\gamma\Delta B_0$ is the difference in precession rate due to magnetic field inhomogeneities. T2 relaxation can visually be displayed (Figure 2.2)
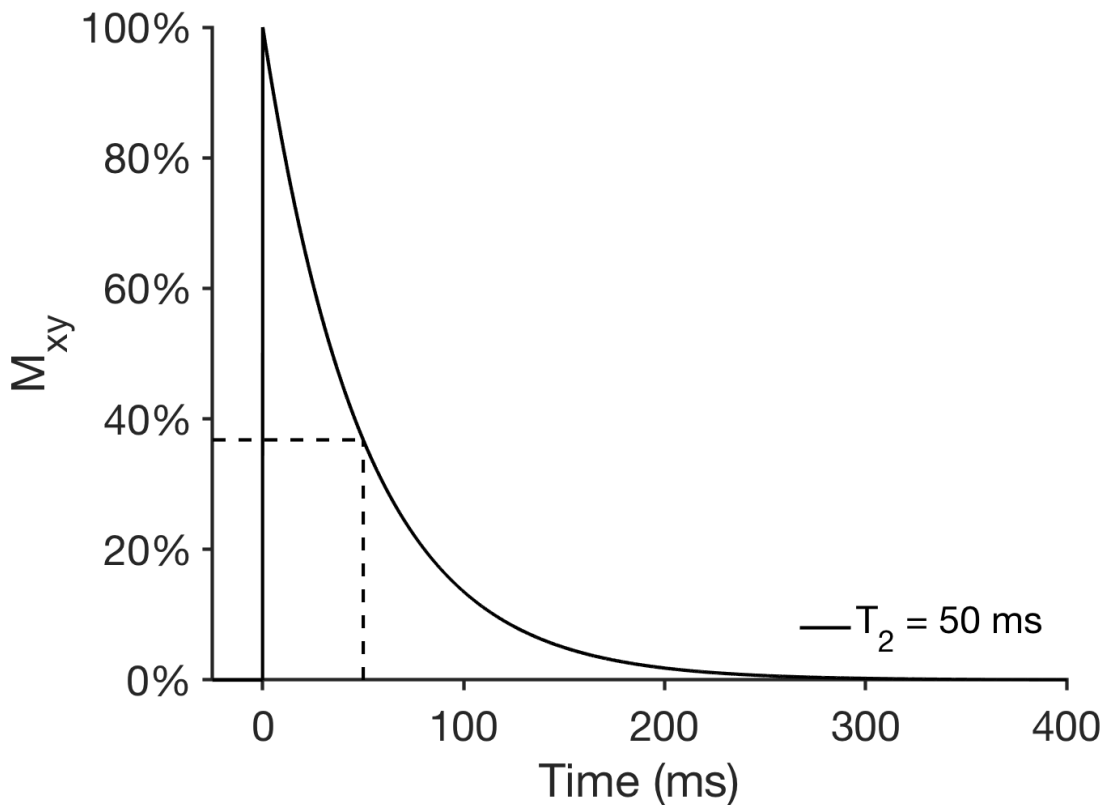
Figure 2.2 Visual representation of T2 relaxation. *The vertical axis shows % of magnetization measured in the xy-plane and the horizontal axis shows time in ms. When the magnetization is brought down to the xy-plane by a 90° radio frequency pulse, the magnetization decays exponentially due to spin-spin interactions as displayed by the curve. T2 is defined as the time when the decay has reached 37% of the initial magnetization, which in this case is at 50 ms. In this case, we assume T2*=T2.*

Simultaneously as the transverse magnetization decays, longitudinal magnetization recovers. After a 90° RF pulse flips the magnetization to the xy-plane, the spins tend to return to their

10

thermal equilibrium around B_0. This leads to the recovery, or regrowth, of the longitudinal magnetization (M_z) along the z-axis [33]. This process is known as T_1 relaxation, or T_1 recovery, and depends on the strength of B_0, the tissue characteristics, and the surroundings. T_1 relaxation is an exponential process with a time constant, which is described by Equation 1.3.

$$M_z = M_0 * (1 - e^{-\frac{t}{T_1}}),$$

where t is the time after the RF pulse, T_1 is the time constant that expresses the time course of longitudinal relaxation until the magnetization vector reaches the initial equilibrium state, M_0 is the original magnetization (in equilibrium before any RF pulse is applied) and M_z is the magnitude of the magnetization along the z-axis. T_1 relaxation can also be visually displayed (Figure 2.3)
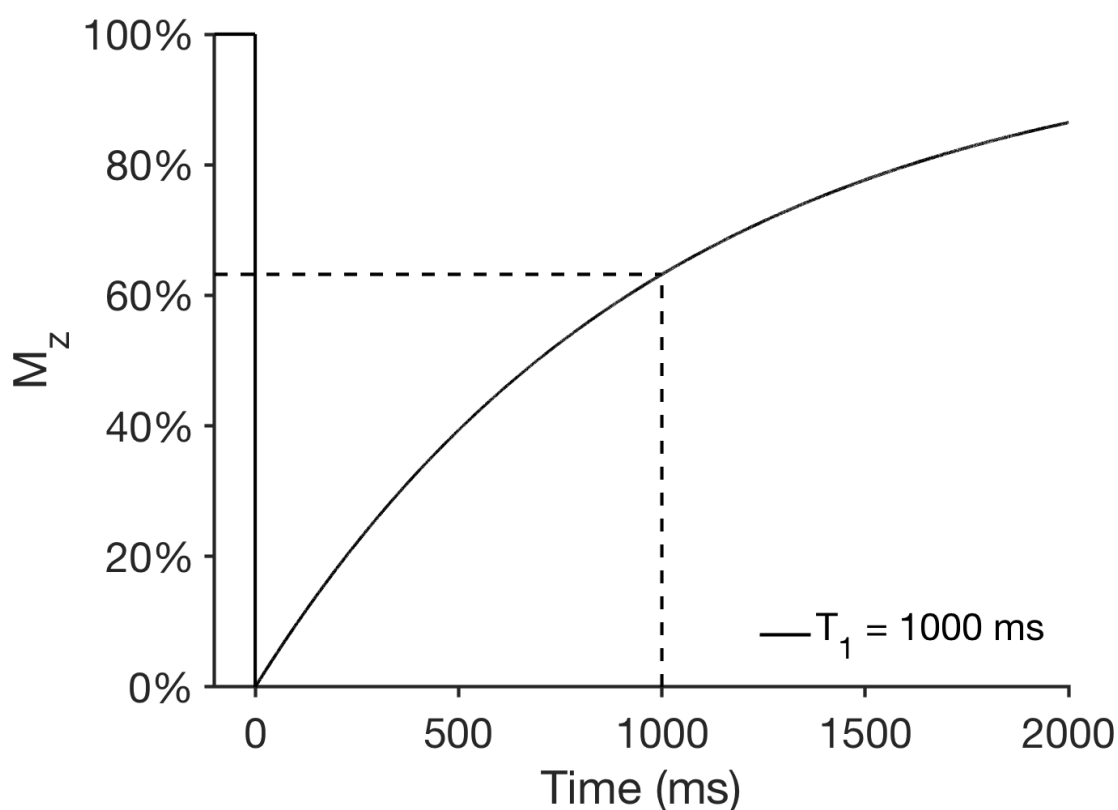
Figure 2.3 Visual representation of T_1 relaxation. *The vertical axis shows longitudinal magnetization in % of initial magnetization and the horizontal axis shows time in ms. After the magnetization is brought down to the xy-plane by a 90° radio frequency pulse, the magnetization, in the z-direction will exponentially recover until its initial magnitude is reached, as displayed by the curve. T_1 is defined as the time when roughly 63% (1-1/e) of the initial magnetization is recovered, which in this case is at 1000 ms.*

The magnitude of the longitudinal magnetization affects the signal intensity (SI) in the images. Fat, for example, has a shorter T_1 (the spins recover faster) than muscle, thus fat appears with a brighter signal in T_1-weighted images. Furthermore, if gadolinium-based

contrast agent is present this will facilitate the dispersion on the spin energy [35], thereby accelerating the regrowth of the longitudinal magnetization, and thus increasing the image signal intensity.

While RF pulses are most commonly used for excitation, there are many more uses in MRI. Most prominent in this work is the inversion pulse, which flips the magnetization along the transverse axis. The simplest design of an inversion pulse is similar to an excitation pulse, but with a 180° flip angle, but more advanced pulses such as adiabatic pulses are common.

T_1 and T_2 relaxation is inherent to every tissue, thereby providing distinctive information about a given tissue due to its composition. This is why MRI can provide detailed images of complex anatomical structures, since the inherent differences in magnetic properties cause image contrast depending on the timing of the RF-pulses.

2.1.3 Location of signal origin

So now we know how an image signal is generated, but how do we know the spatial location from which the received signal originated? In order to form a comprehensive image, the location of any part that is going to be visualized needs to be recorded. Now the third part of the MRI scanner, the gradient coils, work their magic. So called *spatial encoding* is performed by applying magnetic field gradients, using the gradient coils, in order to localize the spatial origin of the signal. As there are three spatial dimensions to consider, there are three encoding strategies that are usually employed; slice selection, frequency encoding and phase encoding.

2.1.3.1 Slice selection

Slice selection is performed by applying a magnetic gradient during the application of the RF pulse, which induces a slight difference in the magnetic field over the subject intended for imaging. The Larmor frequency is directly proportional to the field strength, and a gradient in the field strength will cause the spins to precess at different rates along the gradient. Only the spins with the precession rate of the RF pulse can be excited, which allows for signal recording from the slice selectively without interference from other slices [36].

2.1.3.2 Phase encoding

Once again, gradients are used to affect the phase of the spins, however the phase encoding gradient affect the entire spectrum of the frequency encoding direction. This means that in order to separate the signals' spatial origin, the acquisition needs to be repeated as many times as the wanted number of picture elements in the phase encoding direction. As a consequence, the time needed to acquire an image is dependent on the resolution the phase encoding direction, but not the frequency encoding direction.

2.1.3.3 Frequency encoding

By using the same technique that was used for slice selection, frequency encoding can be accomplished by applying a gradient that changes the frequency of the precession for different space points in one dimension [37]. However, instead of being applied during the RF pulse and interfering with the slice selection gradient, the frequency encoding gradient is applied during what is known as readout. The acquired signal will originate from spins precessing at distinctive rates due to their position along the frequency encoding direction. The Fourier transform, which translates frequencies into locations, can therefore be used to identify the positions of the original signals [36].

2.1.4 Pulse sequences

Now we know the basic principles for signal generation, and how a signal is translated into a diagnostic image with CMR. However, reality is somewhat more complicated, and in practice several RF pulses and gradients are played out in what is known as a pulse sequence, that can be varied in order to depict a certain tissue property or physiological response. In order to fully understand the coming sections, let us go through some important parameters.

- Flip angle (FA) – the angle the magnetization is flipped by an excitation pulse.
- Repetition time (TR) – the time elapsed from one excitation pulse to next.
- Inversion time (TI) – the time from an inversion (180°) pulse to the excitation pulse.

2.1.4.1 T_1-weighted imaging

Image acquisition parameters in a pulse sequence can be selected to enhance the contrast between particular types of tissue. A short TR time allows for water and fat to be distinguished [38]. This is due to that the longitudinal magnetization (T_1) in fat recovers faster than it does in water, subsequently this affects the contrast in T_1-weighted images.

LGE is a T_1-weighted imaging technique that utilizes the difference in distribution of an extracellular contrast agent in normal compared to non-normal myocardium. Late refers to the fact that the images are acquired at least 10 minutes after contrast administration so that the contrast agent has had adequate time to exchange between tissue and blood, achieving a dynamic equilibrium. LGE has become the non-invasive reference standard to visualize and diagnose myocardial cell damage. Gadolinium coupled with diethyelene triamine pentaacetic acid (DTPA) or other similar molecules are referred to as extracellular contrast agents that affect the magnetic properties of the tissues they distribute within. The main effect of the contrast agent is to markedly reduces T_1 values, and thus tissues that have a higher extracellular space will appear brighter on T_1-weighted images.

One way of producing strong T_1 contrast is to use an inversion recovery pulse sequence, which can null a tissue with a particular T_1-time depending on the TI. Clinically, a trial-and-error based methodology is typically used to determine TI for LGE imaging. The operator acquires images with different TIs with a Look-Locker sequence, called TI scout (Figure 2.4).

These images are visually inspected and the operator chooses the TI when it is perceived that the myocardial signal is "nulled", i.e. the myocardium is as black as possible.
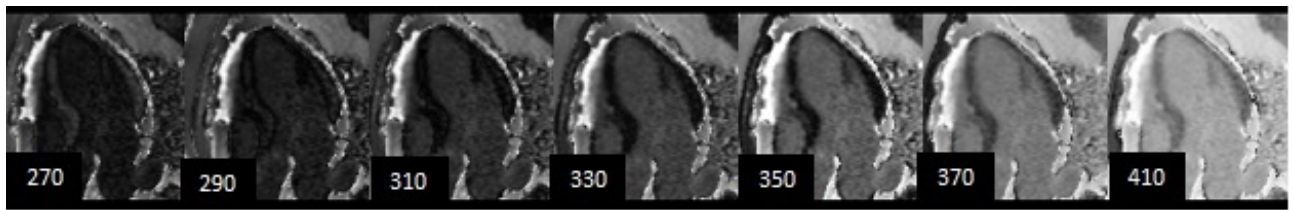
Figure 2.4. Illustration of inversion recovery (ms) in TI scout. *Numbers in the left corner denote TI in ms. Note how the image contrast differs across the different TIs, both in blood and myocardium. The TI scout aims to identify where the normal myocardium is nulled, and appears black. In this particular instance, this happen somewhere around 310-330 ms. If TI was set to 270-290 ms this would be too early, and the myocardium would appear white and with little contrast between blood and myocardium. A TI of 350-410 ms would be too late, the myocardium is too bright, almost grey, and it would be more difficult to separate the endocardium from the blood pool, thus limiting the possibility to identify subendocardial myocardial damage.*

2.1.4.2 T_1 mapping

Instead of merely producing a T_1-weighted image, a technique to quantitatively image and measure the longitudinal relaxation time called parametric pixel-wise mapping has been developed [39]. The T_1 mapping technique inverts the magnetization (flips the magnetization by 180°) by using an inversion recovery (IR) sequence and during the relaxation process, images are acquired at multiple time points (TIs). The images are acquired in late diastole and during an end expiration breath hold. A commonly used T_1 mapping technique is called modified Look-Locker inversion recovery (MOLLI) (Figure 2.5) [39]. The technique samples the recovery of longitudinal magnetization after inversion, the IR curve. Signal intensity over time is used to plot the longitudinal relaxation curve. When the curve is plotted for each pixel in the image, we can solve for T_1, and T_1 can be displayed as a pixel-wise T_1 map. In the T_1 map, T_1 in milliseconds is encoded in the intensity of each pixel. This allows for standardized cut-off values for inter- and intra-patient evaluations.
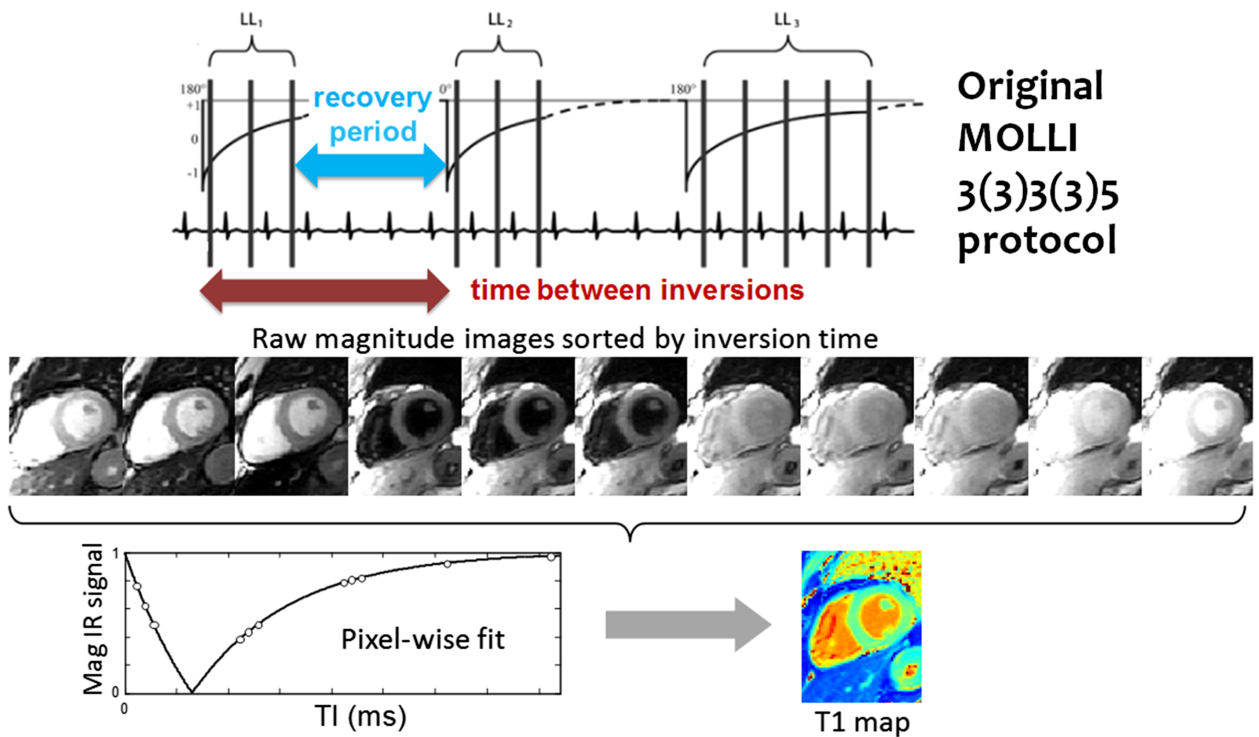
Figure 2.5. Illustration of the modified Look-Locker inversion recovery (MOLLI) scheme. *The schematic displays the original MOLLI protocol used to perform cardiac T_1 mapping. The top figure shows three 180° inversion recovery curves, and the vertical black lines signify readout pulses, which corresponds to end diastole as seen in the ECG curve below. In total, there are three inversions and eleven readouts, and each readout is an image slice acquisition. The time between the inversions and the recovery period are decided by the number of heart beats. The results from the readouts are displayed in the image series below the ECG, which are ordered by inversion times. The pixel-wise relaxation curves from different inversion times are used to estimate T_1 relaxation times and create a map where every pixel in the image corresponds to a specific T_1 value measured in milliseconds. Reproduced from [25].*

2.1.4.3 Phase contrast velocity encoded CMR

Phase contrast velocity encoded CMR is based on that intravascular spins moving along a gradient of a magnetic field will acquire a phase-shift that is directly proportional to flow velocity [40, 41]. By measuring the phase, flow velocity can be derived [42, 43]. By applying first-order gradient moment nulling, or flow compensation, preservation of the phase from areas with flow is ensured. The gradients are then slightly modified to introduce a known phase shift in the spins flowing along this gradient [42-44]. This is known as velocity encoding, which verifies that certain flow velocities are represented by a corresponding phase shift. Since the phase shift is introduced along the velocity encoding gradients, it is worth noting that velocity mapping measures velocity with the respect to the image plane (through-plane velocity), and not velocity in relation to the vessel wall. By subtracting a flow-compensated and a flow-sensitized image, the only remaining phase difference should be due to velocity. However, due to other factors such as eddy currents, additional phase shifts can

be present and causes errors in the velocity measurements. Therefore, correction of zero-phase offset can be performed, in order to ensure accurate display of the flow velocity across the imaging plane. By measuring the phase error in static tissue this can be subtracted from the flow velocities, and this is known as stationary tissue background correction. There are both linear and quadratic stationary tissue background correction methods. The linear correction method assumes that the phase offset errors are spatially dependent in a linear fashion. The method fits a flat surface via the time average of stationary pixels in the velocity-encoded phase images, and the fitted surface is then subtracted from the velocity images. The quadratic correction method performs the fitting of the stationary pixels with a second-degree polynomial assumption. How is stationary tissue identified? Clinically automatic, and semi-automatic methods with manual adjustments are used. The automatic methods identify stationary pixels by a predefined value of the phase deviation over time. The manual adjustments are then employed to include visual static tissue, which can be achieved by changing the threshold for phase deviation and/or by placing a region of interest (ROI) in tissue that should either be included or excluded.

2.1.4.4 Perfusion imaging

Myocardial perfusion can be imaged with CMR by utilizing the dynamic inflow of a bolus of contrast agent. In current clinical practice, a visual assessment of the inflow is used to diagnose the presence of coronary disease. Semi-quantitative techniques have been proposed to mitigate the qualitative assessments, however a quantitative evaluation would be even more desirable. A quantitative perfusion mapping sequence has recently been developed and implemented a fully automated post processing tool using the Gadgetron framework [45]. This technique uses what is known as a dual sequence approach to first pass perfusion. A saturation recovery sequence acquires images at baseline and continuously throughout the first pass of contrast through the myocardium. Low resolution blood pool images are acquired with a fast low angle shot (FLASH) readout, and high resolution images are acquired with a balanced steady state free precession (bSSFP) readout (Figure 2.6). The saturation preparation consists of six non-selective RF pulses where the FAs are tailored by applying gradient spoilers for separation. These images go through extensive post processing for motion correction, identification of the arterial input function, signal intensity normalization and conversion to gadolinium concentration units, deconvolution, and blood flow estimation before finally rendering quantitative pixel-wise color maps of myocardial perfusion [45].
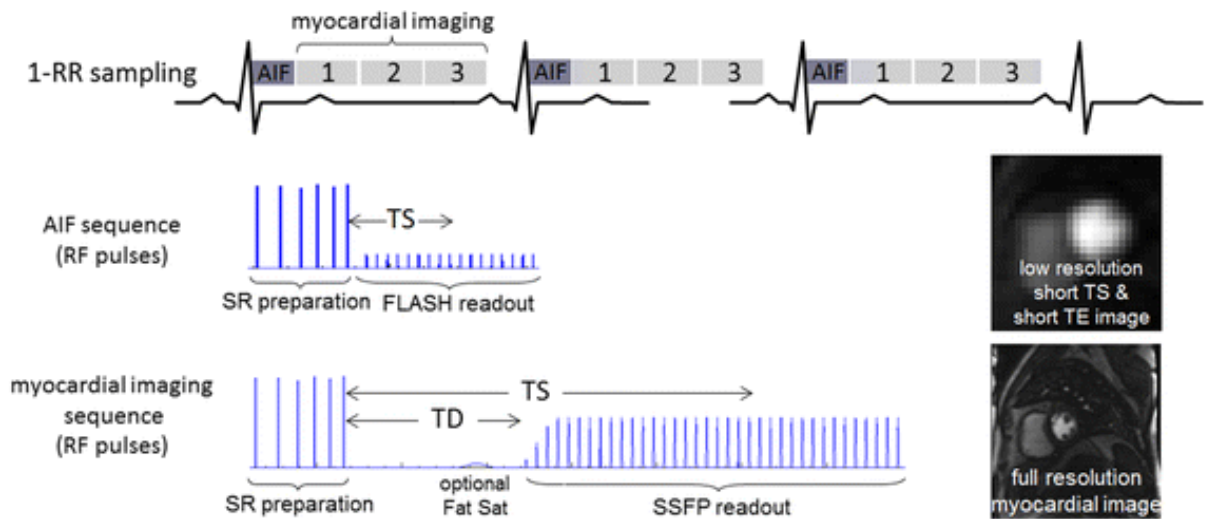
Figure 2.6. Schematic representation of the myocardial perfusion imaging sequence. *The top row shows dual sequence image acquisition in relation to the electrocardiogram (ECG). The first image is the low resolution arterial input function (AIF) acquisition with the RF pulse scheme below the ECG. The following images are high resolution myocardial acquisition with the RF pulse scheme at the bottom. The images to the right show the reconstructed images, at the top the low resolution, AIF image, and at the bottom the high resolution, myocardial image. Reproduced from [45].*

2.2 T_1 MAPPING, ACCURACY AND PRECISION

Native myocardial T_1 mapping has been validated for a comprehensive set of cardiac pathologies such as myocardial infarction [46, 47], myocarditis [47, 48], amyloidosis [49], Anderson-Fabry disease [50], and iron overload [51], and allows for quantitative measurements of tissue characteristics.

The first pixel by pixel T_1 mapping sequence (MOLLI) was introduced by Messroghli, *et al*. [39] and propelled the CMR field to move from LGE as the primary method of tissue characterization. The field has since been exploring the potential of non-contrast tissue characterization using T_1 mapping. As previously described, T_1 mapping samples the IR curve by acquiring multiple images at different TIs to produce a pixel-wise map via curve fitting of the measured values. The TIs are sampled with single shot imaging spaced by the heart beat intervals. In order to acquire the IR curve more evenly, multiple inversions with different trigger delays are employed. This ensures that samples from the entire IR curve are acquired. Multiple inversions introduce a need for a waiting period, to ensure that the magnetization will reach the initial equilibrium. Otherwise, the TIs would be acquired from different recovery curves and compromise the T_1 accuracy and precision. The precision of the T_1 map is therefore linked to the number and the positions of the acquired TIs. The number of acquisitions also affects the accuracy of the T_1 map, as the readout influences the apparent recovery, which affects the signal model used to produce the T_1 map.

2.2.1 Accuracy

The readout used in MOLLI is called steady state free precession (SSFP). SSFP causes the inversion to recover faster and to reach a steady state that is less than the initial magnetization. The time constant describing this sampled recovery curve is referred to as T_1^*, an apparent recovery time constant. The apparent time constant, T_1^*, is less than the actual, desired tissue parameter T_1. To adjust for this accuracy problem the measured values are fitted using an exponential signal model with three parameters. The signal model is described by the equation $S(t) = A - B\exp(-t/T_1^*)$, where t is the inversion time, and T_1^* is the apparent T_1. T_1 is approximated using $T_1 \approx T_1^*(B/A-1)$, and this is called "Look Locker" correction. However, the apparent T_1^* shortening is T_2-dependent, due to the SSFP readout [52, 53]. This means that the T_1 map has a slight T_2-weighting. The T_2 dependent error is also increased by imperfect inversion efficiency, however this can be minimized by using an inversion pulse with a short duration [54]. The T_2 dependency is not all bad, as a 100% increase in T_2 will result in a 4% increase of the T_1^*. For example, in tissues with edema with both increased T_1 and T_2, the T_1^* elevation will be slightly higher, thus improving detectability [25]. However, the T_2 dependency also leads to that T_1 mapping using SSFP readouts is sensitive to heart rate and off-resonance effects.

2.2.1.1 Off-resonance effects

Off-resonance will cause banding artifacts when using the SSFP readout, which is visually apparent to the clinician. However, small off-resonance frequencies that will not cause visual banding artifacts, can still result in a significant error in the T_1 estimate [55]. Regional variation in the B_0 field that surrounds the heart cause regional variations in T_1 that in fact are artifacts. Off-resonance related errors can be reduced by reducing the FA, however, this comes with the cost of lower precision due to a noisier map [25].

2.2.1.2 Heart rate dependency

The heart rate dependency when using MOLLI is related to two major factors 1) the time between inversions and 2) the SSFP readout influence on each inversion recovery. By changing the order of the inversions in the acquisition protocol, the time between inversions can be increased. The SSFP readout effect can be mitigated by reducing the number of inversions. The (3(3)3(3)5) original MOLLI protocol acquired 11 images in 17 heart beats using 3 inversions, and the recovery time between inversions was set to 3 heart beats. It is easy to understand that with higher heart rate, the inversion curves do not fully recovery during 6 heart beats (acquisition + recovery). Thus, the magnetization does not reach initial magnetization equilibrium before the subsequent inversion pulse. Therefore, the 5(3)3 protocol was introduced, to acquired 8 images in 11 heart beats using 2 inversions with the time between inversion set at 8 heart beats [46]. This protocol improved heart rate sensitivity by starting with 5 acquisitions during the first 5 heart beats, followed by a recovery time of 3 heart beats. However, the 5(3)3 protocol was further modified to set the time between inversion in seconds (5(3s)3), which furthered mitigated heart rate dependency [56]. By

18

adjusting the protocol to determine both acquisitions and time between inversion in seconds, and not heart beats, a more complete recovery at high heart rates is ensured (5s(3s)3s) [25].

Another strategy to deal with the heart rate dependence, known as ShMOLLI, was introduced in 2010 [57]. The (5(1)1(1)1) protocol acquires 7 images in 9 heart beats during 3 inversions, and performs conditional fitting. This means that in pixels with long T_1 measured during a short RR interval, data will be refitted using only the first 5 measurements acquired during the first inversion. The protocol reduces heart rate dependency, however it also introduces a loss of precision associated with discarding data.

2.2.1.3 A new approach for absolute accuracy

An alternative to IR is saturation recovery (SR). With SR approach, each recovery becomes independent of the others, and recovery periods become obsolete. Therefore, saturation recovery single shot acquisition (SASHA) was developed [58]. Similarly to the MOLLI protocol, multiple time points are obtained however SASHA acquires images of the saturation recovery curve and performs a pixel-wise curve fit (Figure 2.7). The SR curve recovers according to T_1 relaxation, but the magnetization recovery is not as influenced by the SSFP readout as the IR curve. This eliminates several sources of inaccuracies compared to IR techniques as no correction of the T_1^* has to be performed. Therefore, SASHA has a better accuracy compared to MOLLI-based techniques. However, SASHA is acquired with a higher FA and the SSFP readout slightly alters the shape of the saturation curve. This is accounted for with either a 2- or 3-parameter signal model, which adds an issue of loss of precision [25].
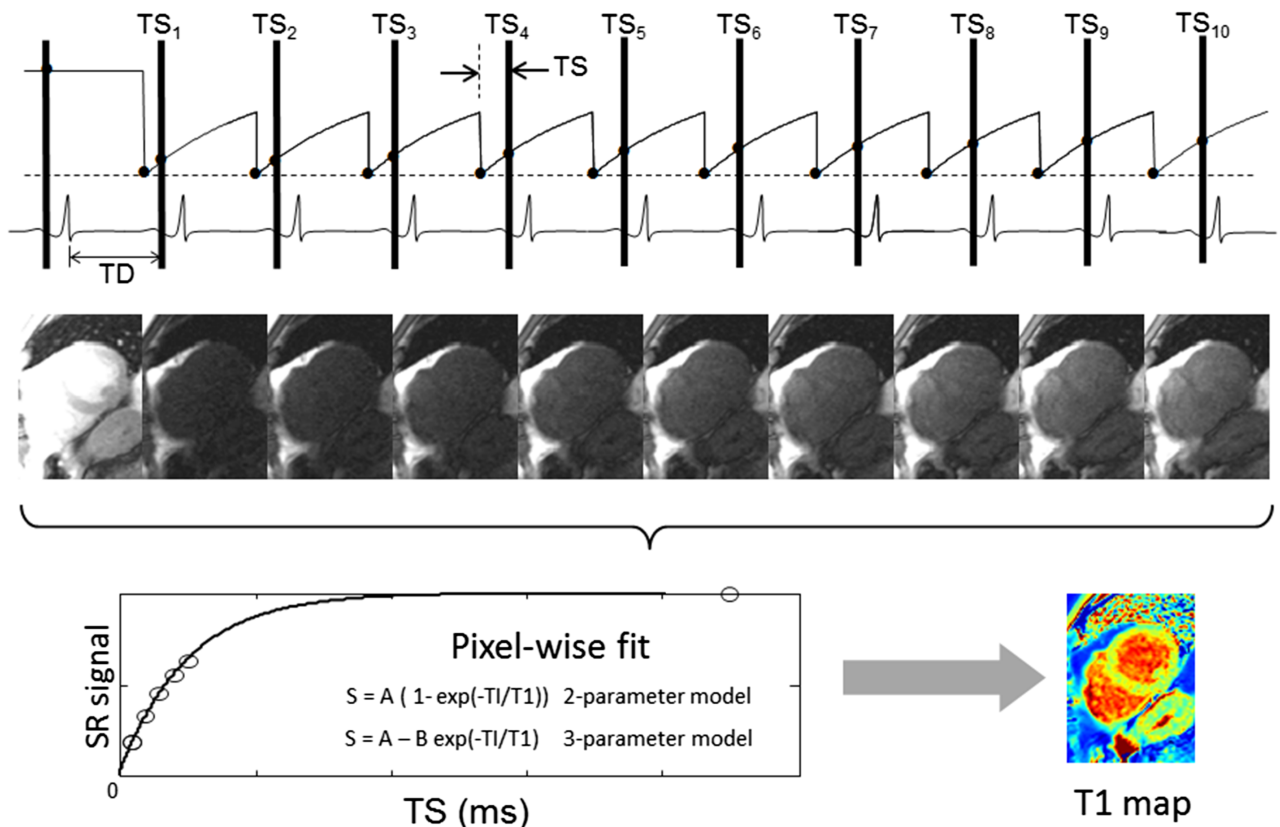
Figure 2.7. Scheme of saturation recovery single shot acquisition (SASHA) protocol.
This schematic displays the SASHA protocol for cardiac T_1 mapping. The scheme starts with a single image acquisition without saturation and followed by image acquisitions at different saturation recovery times (TSi), indicated by the black vertical lines. To ensure mid- to end-diastolic imaging are all the images acquired using an equal delay from the R-wave rigger (TD). The different TSi are used to plot a T1 relaxation curve and a pixel-wise fit is performed to produce a T_1 map where every pixel value in the image corresponds to a specific T_1 time measured in milliseconds. Reproduced from [25].

2.2.2 Precision

The original MOLLI scheme has excellent precision, however the accuracy degrades with higher heart rates [39]. The MOLLI 5(3s)3 also has excellent precision, and the accuracy is less heart rate sensitive. The 5s(3s)3s MOLLI scheme has the same precision as the 5(3s)3 at heart rate 60 beats per minute, but with the advantage of a higher precision at higher heart rates. The ShMOLLI scheme discards data and sacrifices approximately 30% in precision without a gain in accuracy [25]. Precision can be improved furthered in the MOLLI schemes by using phase sensitive inversion recovery (PSIR) reconstruction. The precision of MOLLI is increased with around 30% using PSIR reconstruction compared to multi-fit magnitude inversion recovery fitting [59]. SASHA acquired during a breath hold duration identical to a MOLLI 5(3s)3 protocol will have a higher accuracy, however a degraded precision compared to the MOLLI protocol. The loss of precision is around 35% for SASHA with a 2-parameter fit compared to 5(3s)3 MOLLI. With SASHA using the 3-parameter fit the loss of precision is 125% compared to 5(3s)3 MOLLI with 3 parameter fitting [25].

2.2.3 Improving T_1 mapping

Different approaches to optimize T_1 mapping include changes in the imaging protocol to circumvent heart rate dependency and reduce the duration of breath hold [57, 60], motion correction to reduce the effect of respiratory motion for patients with poor breath holding [59], PSIR reconstruction to improve measurement precision [59], and saturation based techniques for higher accuracy [58]. However, as we learn more about the factors influencing the accuracy and precision of T_1 mapping [61] new areas of improvements arise such as blood correction, and the potential use of T_1 mapping for scar imaging.

2.2.3.1 Blood correction

Approximately 4-5% of the left ventricular stroke volume in healthy humans enters the coronary arteries and perfuse the myocardium [62]. The T_1 value of blood is much higher (around 1400-1700 ms) than the T_1 value of myocardium (900-1100 ms), shown in our own data at 1.5 T. Since the myocardium contains blood, the myocardial T_1 value is likely to be influenced by the T_1 values of this blood volume. Thereby, T_1 value of the intramyocardial blood may obscure the true T_1 values of the cardiomyocytes. Since different diseases may

20

influence both the amount of blood in the myocardium, but also the T_1 value of blood, these processes might weaken clinical diagnosis based on T_1 mapping.

The partial volume effect is the concept that a one voxel might comprise of different tissues, or a tissue of different features, where the pixel value for the voxel reflects the average of these contents [63]. Furthermore, the myocardial T_1 values reflect a tissue consisting of cardiomyocytes, extracellular connective tissue, signal transductions connections, blood vessels with blood inside [64, 65]. Therefore, myocardial T_1 values, should be related to the entire composition of this tissue, which also includes the microcirculation. The blood T_1 values vary due to several factors such as hematocrit [66], HDL cholesterol, iron [67], pH, temperature, sex [60], age [68] and oxygen pressure [66, 69]. Variations in these different characteristics may therefore influence the evaluation of myocardial T_1 values. Several approaches for correcting the myocardial T_1 values for blood T_1 values have been reported [70, 71]. Reiter, et al. [71] eliminated age and sex differences when correcting myocardial T_1 values, for T_1 values measured in the LV blood pool. Therefore, performing blood correction could increase the precision of native myocardial T_1 values between patients. This could furthermore improve the accuracy of clinical T_1 mapping and reduce the sample size needed for clinical research. However, it is unknown which parameter to use for blood correction, and furthermore any potential blood correction model needs to be validated in a separate cohort.

2.3   DIAGNOSTIC PRECISION IN FLOW QUANTIFICATION

CMR flow quantification for determining the ratio of flow between the pulmonary and systemic circulation (Qp/Qs) is used to quantify cardiac shunts. However, measurement errors may influence both the accuracy and precision of the flow quantification. Therefore, post-processing corrections algorithms have been proposed to reduce measurements errors [21]. These methods include both linear and stationary tissue background correction, which have not been evaluated systematically, and it is currently not known how the correction algorithms affect clinical precision and accuracy. In the clinical setting, there are different software implementations in use. However, how these software products perform with regards to precision and accuracy is unknown. It is therefore of importance to elucidate whether the clinical software algorithms actually improve clinical evaluation, and furthermore understand how they perform in relation to each other. Also, a number of patient characteristics might influence the background correction such as body surface are or image angulation. The different characteristics need to be investigated for changes in accuracy and precision of Qp/Qs after background correction, in order to understand which patient benefits from stationary tissue background correction.

2.4   IMAGING OF FOCAL LESIONS

Myocardial cells are irreversibly damaged during an acute myocardial infarction when they lose their cellular integrity after cell membrane rupture [72]. Intravenous injection of gadolinium distributes into the extracellular space of what before an acute myocardial

infarction, would have been the intracellular space of cardiomyocytes [73, 74]. Furthermore, gadolinium distributes in the extracellular space of tissues with increased amount of extracellular matrix or fluid [35] Therefore, the LGE sequence can be used to visualize non-ischemic diseases with either fibrosis, or high-grade inflammation. Gadolinium enhances the contrast of the damaged tissue from the normal myocardium, and LGE images will visualize focal myocardial fibrosis, regardless of its origin (Figure 2.8). The underlying etiology can be determined from the pattern of enhancement, since the ischemic focal myocardial fibrosis involves the subendocardial layer of the LV myocardium and is restricted to the perfusion territory of the relevant coronary artery. Epicardial focal fibrosis that does not include the endocardial layer can be caused by several infectious, inflammatory and other myocardial pathologies [13].
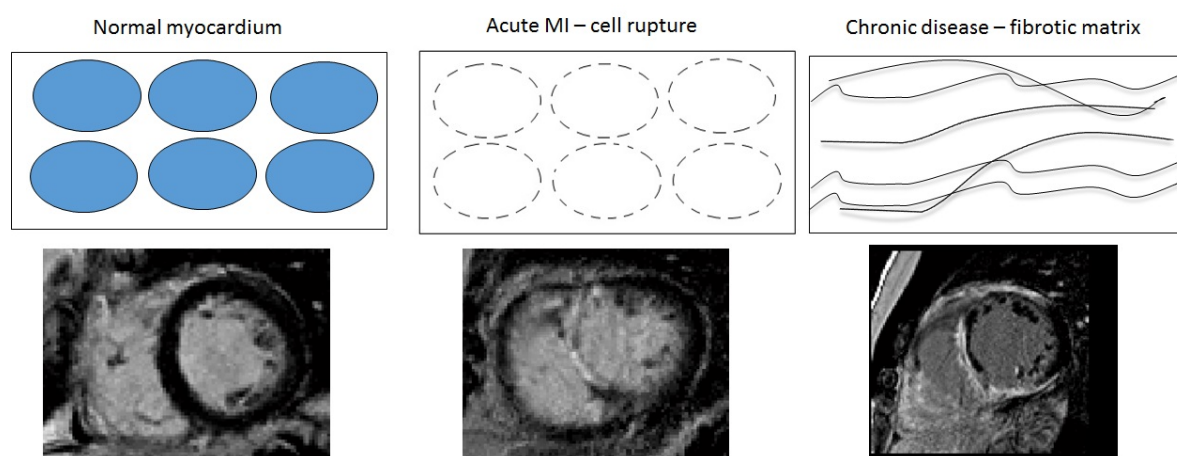
Figure 2.8. The gadolinium enhancement in different disease states. *Simplified schematic illustration of gadolinium distribution in different tissues, and how this appears in LGE images. The top row shows images of the cellular tissue level. The bottom row shows corresponding LGE images. The left panel shows normal myocardium with intact cell membranes. The middle panel shows an acute myocardial infarction (MI) with cell membrane rupture. The right panel displays an inflammatory disease with a fibrotic collagen matrix. Notice the pattern of enhancement in the middle picture; an acute myocardial infarction with transmural extent, distributed from the endocardium to the epicardium in the septum. The right LGE image illustrates a non-ischemic disease, sparing the endocardium, with only epicardial focal fibrosis. Both myocardial lesions of the middle and right images involve the septal part of the myocardium, the wall between the right and left chambers, separating the blood pools from each other. Adapted from [75].*

However, the TI that needs to be set for LGE acquisition differs between patients and even in the same patient over time, due to renal clearance of the contrast agent, differences in contrast dose, the time elapsed after intravenous contrast administration, the habitus of patient's body and cardiac function [76]. This inherent methodological factor can become a challenge during clinical imaging. The LGE image is dependent upon relative differences in signal intensities between focal myocardial damage and normal myocardium [77, 78]. However, diffuse

fibrosis may be missed by LGE, since the signal intensity may be close to isointense, which causes all the diseased myocardium to be nulled and perceived as healthy myocardium. The clinical evaluation of these images, and the patient's diagnosis is dependent on the observer's visual discriminative ability.

Quantitative T_1 mapping can be used to detect both focal and diffuse myocardial pathologies [48, 49, 79]. Myocardial T_1 values that are measured following the injection of gadolinium can convey information about both focal myocardial fibrosis, but also additional information about the extracellular volume fraction (ECV) though the production of ECV maps [46, 80]. Notably, it is not possible to quantify ECV using LGE images. Post-contrast T_1 maps may be used to appreciate the expansion of the myocardial extracellular space [39]. However, post-contrast myocardial T_1 values vary according to the injected dose of contrast, renal clearance, time of acquisition, body composition and hematocrit, like in the case with LGE [75]. Therefore, myocardial T_1 values measured post-contrast for distinguishing diseased from normal myocardium suffers from limited precision [81]. However, synthetic LGE (SynLGE) images can be generated using post-contrast T_1 maps, with an image contrast similar to conventional LGE images. Both post-contrast T_1 maps and LGE images are currently acquired during a clinical scan. If SynLGE images visually provide the equivalent diagnostic information regarding focal myocardial fibrosis compared to LGE, LGE acquisition could be omitted from the examination. However, it is currently unknown if SynLGE can provide equivalent diagnostic information regarding focal myocardial fibrosis compared to conventional LGE. Furthermore, the sensitivity and specificity of SynLGE compared to conventional LGE in terms of detecting focal myocardial fibrosis need to be investigated, which we performed in Study IV.

3 DIFFERENCES IN CARDIOVASCULAR DISEASE BETWEEN THE SEXES

Over the last 20 years, mortality in cardiovascular disease in Sweden has been cut in half. However, this reduction has been more pronounced in men than in women [82]. Some diseases have a higher prevalence in women, including myocardial infarction with non-obstructive coronary arteries (MINOCA), Takotsubo cardiomyopathy but also pulmonary hypertension [83]. Differences between the sexes in cardiovascular disease are multifactorial, and include both gender- and sex-related factors.

3.1 SEX DIFFERENCES IN CARDIOVASCULAR PHYSIOLOGY

Several differences in the cardiovascular system between women and men exist. Men have higher cardiac output, an average of 5.6 l/min, compared to women, with an average cardiac output of 4.9 l/min [62]. However, when accounting for body surface area by using the measurement cardiac index the sex differences disappears [84]. The cells that enables transport of oxygen to the body are called red blood cells (RBC), and contain hemoglobin. The average number of RBCs per mm^3 of blood in men is 5 200 000 ($\pm$300 000), whereas in women it is 4 700 000 ($\pm$300 000). The amount of hemoglobin (the molecule that binds oxygen in the RBCs) also differs between the sexes. Whole blood in men contains on average 15 g of hemoglobin per 100 ml of cells, which is slightly lower in women, with an average of 14 g per 100 ml of cells. One gram of hemoglobin can carry 1.34 ml of oxygen. This means that a healthy man can carry a maximum of 20 ml of oxygen per 100 ml of blood, whereas a woman can carry 19 ml of oxygen per 100 ml of blood at maximum [62]. Furthermore, younger women have higher heart rate compared to men. The heart rate variability is also higher in women compared to age-matched male controls. However, the differences between the sexes disappears in their fifties [85]. The heart rate variability decreases with age, however, this decrease in more pronounced in men. A difference in heart rate variability in women can only be seen when comparing the youngest (10-29 years) to the oldest (70-99 years) [85]. Women's hearts also have a smaller mass compared to men, as well as lower volumes [86, 87].

3.2 ISCHEMIC HEART DISEASE

Ischemia is defined as an insufficient blood supply to a tissue in relation to demand, and thereby not fulfilling the need for oxygen in the specific tissue. Ischemia is usually caused by a restriction of the blood flow, and in the coronary arteries specifically, it can be caused by a complete blockage (occlusion) or a reduction in blood flow (stenosis). The underlying pathology for ischemia in the heart is usually an atherosclerotic process within the coronary arteries, causing a narrowing of the vessel which eventually restricts flow of blood to the heart muscle downstream from the affected site [88]. This narrowing, the atherosclerotic plaque, may rupture, exposing the underlying layer, which causes a blood clot to form on site, that completely blocks the coronary artery [89]. This complete blockage causes acute

myocardial ischemia. If this blockage is not resolved, prolonged ischemia will progress to irreparable cell death within 2-4 hours, and the formation of a myocardial infarction over the course of 5-6 weeks [72]. It is known that the degree of atherosclerotic obstruction does not predict the risk of plaque rupture, and it is possible to develop complete coronary occlusion and consequent acute myocardial infarction (AMI) without any preceding symptoms [90, 91]. Thereby, a stenosis does not always rupture, instead it can progress continuously until it restricts blood flow when the oxygen demand is increased i.e. during physical activity [92]. Ischemic heart disease has therefore historically been divided into two subgroups: acute ischemic heart disease and stable ischemic heart disease.

3.2.1 Sex difference in acute ischemic heart disease

Around 30 000 people are diagnosed with AMI every year in Sweden. A third of those diagnosed with AMI are women. The average age for men that are being treated for an acute myocardial infarction at the coronary care unit (CCU) is 71 years, whereas it is 77 years for women. In women with AMI, it is more common that there is no significant stenosis or completely normal coronary arteries present when undergoing angiography. This is called MINOCA (myocardial infarction with non-obstructive coronary arteries) and MINCA (myocardial infarction with normal coronary arteries). Even though the most common pathology for AMI is obstructive atherosclerotic plaque there are atherosclerotic plaque that can hide in the vessel wall [93], and these plaques can erode (bleed) [94, 95]. Plaque-erosions are more common in women, and it has been speculated that this may cause distal clotting, which could be a possible pathogenesis for MINOCA [96].

A difference between the sexes that is likely gender related is the difference in symptom of acute ischemic heart disease. The most common symptom of AMI is central chest pain that can spread to the left arm or both arms, to the neck and jaw and sometimes to the back. However, 40% of all women with ACS (AMI and instable angina) do not present with chest pain. Instead they experience other symptom such as shortness of breath, nausea and fatigue. Women with ACS more often than men experience several symptoms, making the chest pain seem less prominent.

3.2.1.1 *Sex differences in diagnosis of acute ischemic heart disease*

Acute ischemic heart disease is also called ACS, and has historically comprised of three clinical manifestations: ST elevation myocardial infarction (STEMI), non ST elevation myocardial infarction (Non STEMI) and unstable angina. The terms ST elevation and non ST elevation originate from how the myocardial ischemia manifests on the electrocardiogram (ECG). ECG is a cheap, fast, and highly accessible test to determine the presence of myocardial ischemia, and therefore one of the major sub classifications of acute ischemic disease is based on the appearance on the ECG. The term angina originates from angina pectoris, which means chest pain, and has become a common term to describe chest pain of cardiac origin.

- ST elevation myocardial infarction (STEMI) originates from the relative rise in the so called ST-segment in the normal ECG, which is located between the S-wave and T-wave. An ST elevation is a sign of transmural ischemia due to occlusion of a coronary artery. If left untreated, the ischemia will developed into a myocardial infarction [97].
- Non-ST elevation myocardial infarction (Non STEMI) includes all aspects of myocardial cell death caused by ischemia with no ST-segment elevation present on the ECG. Inherently this includes a broad spectrum of small ischemic injuries to severe ongoing myocardial ischemia [98].
- Myocardial ischemia that induces symptoms but not cell death is called stable or unstable angina. Clinically, these are separated from manifestations causing cell death (STEMI/Non STEMI) by biomarkers of myocardial cell death in the patients blood (troponins), whereas stable and unstable angina are differentiated via the character of the symptoms [98].

The criteria for diagnosing AMI is an increase and dynamic response in biomarkers of myocardial cell death (troponins) together with at least one of the following criteria [72]:

- Typical symtoms of myocaridal ischemia (acute chest pain) for more than 15 minutes, or lung edema without any other plausible explanation.
- Pathological Q-wave in the ECG.
- Newly developed changes in the ECG associated with myocardial ischemia (i.e. ST elevation or depression)
- Signs of myocardial cell death or regional wall motion disturbance with cardiac imaging.

Men tend to have higher levels of troponins compared to women [99], which could be a reflection of their increased myocardial mass [100]. This sex difference could be a reason to have separate cut-off values for males and females in order to increase diagnostic precision, however, there is currently no consensus [101].

There are different cut-off values for men and women to define an ST elevation using the ECG. For women, a 0.15 mV in the leads V2-V3, and 0.1 mV in the other leads are deemed an ST elevation. However, for men, the cut-off values depend on age, where young men (under 40 years old) can have up to a 0.25 mV elevation in leads V2-V3. However, in older men (over 40 years old) only 0.2 mV in leads V2-V3, and 0.1 mV in the other leads is deemed an ST elevation.

3.2.2 Sex differences in stable ischemic heart disease

The most common symptom of CAD is chest pain during physical exertion, also known as angina. However, approximately one-third of symptomatic patients do not have obstructive CAD [102]. Nevertheless, these patients may suffer from substantial myocardial ischemia, with a poor prognosis [103]. Historically all diagnostic tests for CAD, regardless if they are anatomical or functional, have been developed for the purpose of identifying obstructive

CAD, and have been validated against the coronary angiogram. Given that the clinical focus has been directed towards obstructive CAD, there is now a lack of clinical evidence and knowledge on how to identify and manage patients with angina without obstructive CAD. The first step to bridge this gap is to adopt a unifying terminology. The following terminology has been purposed by Colin Berry [104]:

Ischemic heart disease includes**:**

- **Stable coronary symdrome**
  - Obstructive CAD
  - Ischemia and no obstructive coronary artery disease: *INOCA*
- **Acute coronary syndrome**
  - STEMI
  - Non STEMI/unstable angina
  - Myocardial infarction with non-obstructive coronary arteries: *MINOCA*

The following section on sex difference in stable coronary syndrome will reflect that the current knowledge on INOCA, which is also referred as microvascular dysfunction, is sparse, and that the clinical focus has been on obstructive CAD.

The most common symptom of obstructive CAD is angina during physical exertion. However, there are also atypical symptoms including shortness of breath, nausea and fatigue. Women and older patients more often present with what is called atypical symptoms, making it less likely that the clinician will suspect CAD as the primary cause. A gender aspect of symptoms is that women tend to describe their symptoms as a more diffuse pressure, and not as chest pain [105].

3.2.2.1   *Sex differences in diagnosis of stable coronary syndrome*

There are several diagnostic tests to determine if a patient with chest pain suffers from obstructive CAD. The current guidelines of stable CAD recommend basic testing in the form of ECG at rest, blood samples and echocardiography [106]. In patients with normal LV function, the continuing course of action is dependent upon the PTP. Patients with intermediate risk (15-85%) are candidates for non-invasive testing, where patients in the lower interval are candidates for exercise testing or CCTA, whereas patients with higher risk (66-85%) are eligible for non-invasive imaging including stress echocardiography, SPECT, PET or stress CMR depending on local availability and expertise. Patients with high risk (over 85%) should be assessed with an invasive angiogram, and not wait for a non-invasive test.

Exercise test

The exercise test, in Sweden, is usually conducted on a bicycle ergometer, with the intent to physiologically induce myocardial ischemia. Several parameters are evaluated during an exercise test such as symptoms, maximum work capacity, ST changes and hemodynamic

28

response. Exercise-induced angina in women does not predict future coronary events, and is as common in women with no obstructive CAD as in women with triple vessel disease [101]. However, the angina may be due to INOCA, and may therefore be missed by the anatomical assessment with an angiogram.

The reference values for men and women are different for maximum work capacity, where men are expected to perform at a higher level compared to women. Furthermore, work capacity decreases with age. Therefore, the work load has to be adjusted for every patient, and women more often start on a lower workload compared to men.

Evaluating the ST reaction can pose a challenge in women due to preexisting disturbances in the ST region. There are several contributing factors such as the presence of breast tissue, estrogen levels and valve anomalies. A recent study that compared CCTA to exercise testing in women showed that exercise testing failed to identify obstructive CAD in over half of the patients [107].

SPECT

SPECT is NM technique where a radioactive isotope tracer is injected into a vein (blood vessel), both at rest and during stress (exercise test or with pharmacological stressors). The tracer used for myocardial perfusion imaging will follow the blood stream to the heart, where it is taken up in mitochondria in the myocardium. The parts of the myocardium that are not perfused by blood will appear as a perfusion defect when the images of tracer distribution are acquired. If there is a fixed defect (the defect is present both at rest and stress) it is likely due to a myocardial injury, such as a myocardial infarction. A reversible defect (present during stress, however not during rest) is most likely due to obstructive CAD. There is a risk that breast tissue in women induces an artifact that can be perceived as a defect. SPECT has a high sensitivity for single vessel disease, which is more common in women, however, SPECT cannot identify balanced ischemia or INOCA.

Stress echocardiography

Myocardial ischemia is identified as decreased wall motion, or contractility, at echocardiography during stress. Stress can be induced by physical exertion or pharmacological stress, most commonly using dobutamine. Stress echocardiography is known to be highly operator dependent.

CT

There are two ways to use CT for detecting CAD, one is the calculation of coronary calcification [4] and the other by performing a contrast-enhanced CCTA [5]. Increased coronary calcification increases the risk for future adverse cardiac event, such AMI. The method has a high sensitivity for detecting atherosclerosis, however the specificity for identifying obstructive CAD is low. CCTA provides anatomical information such as plaque morphology but also degree of obstruction. It has a high NPV and therefore, in the UK it is

recommended to perform CCTA as the first-line of diagnostic tests in angina patients without prior coronary disease [108]. However, a CCTA strategy does not increase quality of life nor decrease symptoms compared to standard care [109]. Furthermore, CCTA does not provide information on microcirculation, and therefore inherently lacks the ability to identify patients with INOCA.

PET

PET detects the first-pass perfusion of radioactive tracers with high first-pass extraction and use time-intensity curves and different tissue compartment models to quantify absolute myocardial perfusion (ml/min/g). Myocardial perfusion at rest and stress is used to calculate CFR which can be used for both identification of coronary stenosis and microvascular dysfunction [110]. The main disadvantages of PET are limited spatial resolution, ionizing radiation and clinical availability.

3.3   SEX DIFFERENCES IN PERFUSION USING CMR

Obstructive CAD and several non-ischemic heart diseases effect the myocardial microcirculation [111]. In order to diagnose obstructive CAD or other diseases that alter myocardial perfusion, imaging techniques using pharmacological stressors have been developed [112]. PET is the current reference standard for quantification of myocardial perfusion in ischemic heart disease [113]. However, CMR has potential advantages over PET since it is a method free of ionizing radiation, has better spatial resolution, and is more widely available. CMR can quantitatively measure myocardial perfusion and MBV at rest and during pharmacological stress [20, 113, 114]. However, several CMR approaches for assessing perfusion and MBV exist, including contrast enhanced first-pass perfusion imaging, phase contrast velocity-encoded coronary sinus flow (CSF) measurement, T_1 mapping and ECV imaging, before and during adenosine stress. Decreased MBV reserve during pharmacological stress has been shown to be proportional to the severity of a stenosis of a coronary artery [20, 115]. Recent developments allow for quantitative assessment of myocardial perfusion and myocardial blood volume using CMR [45]. The ability to quantify absolute myocardial perfusion allows for quantification of CFR, which potentially can be used to identify INOCA, as well as obstructive CAD. However, it is important to investigate if any sex differences exist in normal physiology, as normal ranges might differ between the sexes. It is important to identify any potential differences in order to introduce proper cut-off values when moving towards quantification, which will increase both the accuracy and precision of a newly developed method.

4 AIMS

The overall aim of this thesis was to identify parameters that affect clinical diagnostic precision, as well as sex differences that influence clinical evaluation in a variety of different CMR methods.

The specific aims for each study were:

1) To investigate the impact of intramyocardial blood on native myocardial T_1 values. This included identifying which blood parameter that had the biggest effect on the myocardial T_1 values, constructing a blood correction model, and validating the correction model for clinical use.

2) To evaluate the changes in precision and accuracy following stationary background tissue correction in phase velocity encoded CMR flow quantification. This included elucidating if any particular parameter such as sex, or hematocrit affected the background tissue correction and thereby, could affect the clinical interpretation of the pulmonary-to-systemic blow flow ratio.

3) To explore if sex differences in myocardial perfusion, myocardial blood volume and extracellular volume exists

4) To analyze the diagnostic value of synthetic scar imaging from post-contrast myocardial T_1 mapping.

5 MATERIALS AND METHODS

5.1 STUDY POPULATIONS

In three of the four studies (Study I, II and IV) the study populations consisted of consecutive clinical patients referred for CMR at Karolinska University Hospital, Stockholm, Sweden, between different predefined dates, which will be described in greater detail below. There was an overlap between the study populations of Study I and Study II, where a total of 18 patients fulfilled the inclusion criteria to be included in both studies. In Study I, a population of healthy volunteers from University College London was also included. The study population in Study III consisted of a prospective cohort of healthy volunteers from Karolinska University Hospital. Ethical approval was granted for all study procedures, and all subjects provided written informed consent.

5.1.1 Study I

In total, 400 consecutive patients scanned between January 2014 and August 2015 were retrospectively enrolled. The goal was to include 200 females and 200 males respectively, and the inclusion was terminated when the goal was met. Exclusion criteria and the number of excluded patients can be found in Figure 5.1

Healthy volunteers (n=77) were prospectively enrolled between April 2014 and July 2015. The volunteers were included if they had no cardiovascular disease or diabetes.
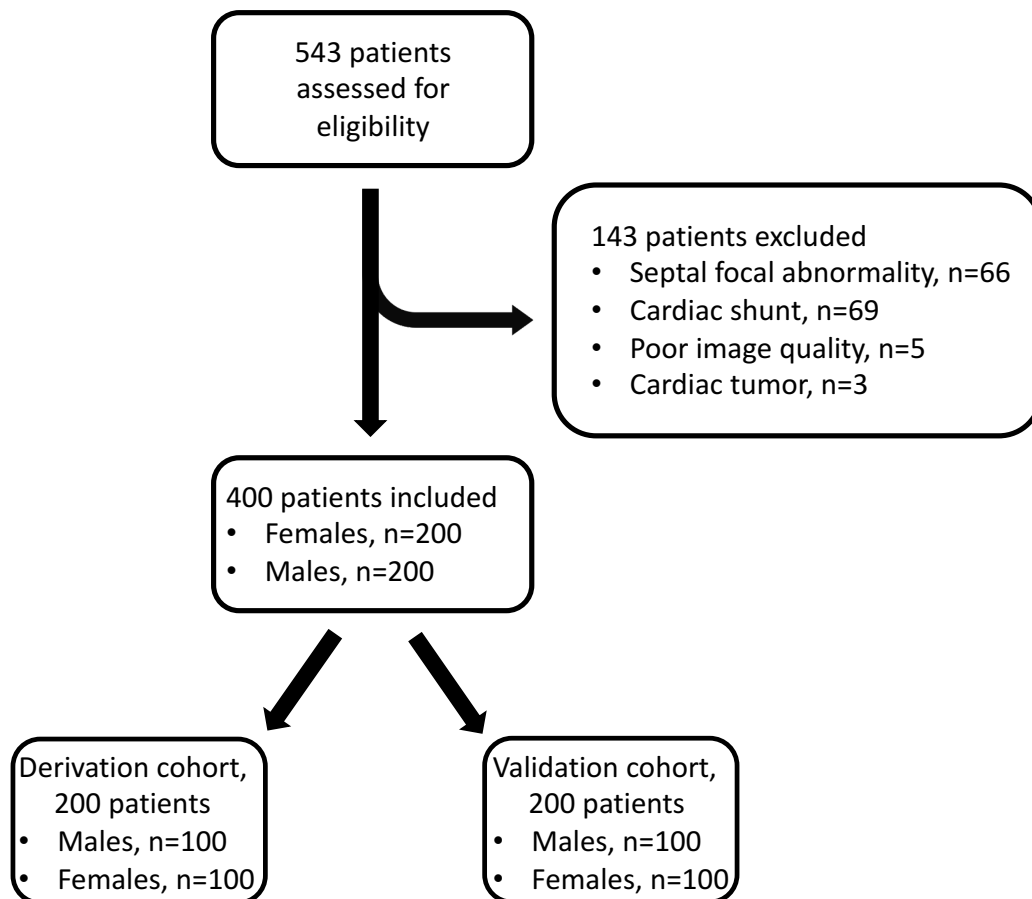
Figure 5.1 Patient population. *The flow chart displays patient inclusion, exclusion and final constitution of the respective derivation and validation cohorts.*

5.1.2 Study II

Consecutive patients (*n*=91) referred for clinical CMR, examined between January and September 2014, were retrospectively enrolled. Inclusion criteria included that the clinical report had no mention of cardiac shunt or malformations of the great vessels, no persistent arrhythmias defined as a standard deviation of the mean R-R interval during flow image acquisition exceeding 10% or the R-R interval for either acquisition, and no poor image quality due to extensive fold over.

5.1.3 Study III

Healthy volunteers (*n*=43) with no cardiovascular medication, no history of asthma, no history of cardiovascular or kidney disease, that were current non-smokers and had a normal 12-lead ECG were included. Exclusion criteria included failed splenic switch off [116], low AIF (<2mmol/l), and poor image quality.

5.1.4 Study IV

A total of 109 clinical patients referred for diagnostic CMR assessment of known or suspected heart disease between February 2012 and October 2013 were retrospectively identified.

5.2 IMAGE ACQUISITION AND ANALYSIS

All patients in Study I, II and IV, and healthy volunteers in Study III were scanned on a 1.5 T system (Magnetom Area) with an 18-channel body matrix coil, together with a spine matrix coil. All scans were performed with the subject in the supine position. The healthy volunteers in Study I were scanned on a 1.5 T system (Magnetom Avanto) in a supine position, with a 32-channel cardiac phased array receiver coil. Patients in Study I were analyzed using SyngoVia VA30 (Siemens), and a clinical work station (ISD7, Sectra). Patients in Study II and IV, and healthy volunteers in Study III were analyzed using SyngoVia VA30 and Segment (Medviso AB)[117]. Healthy volunteers in Study I were analyzed using CVI42 software (Circle, Cardiovascular Imaging Inc.).

5.2.1 Study I

All patients had acquired native myocardial T_1 maps using a 5(3)3 modified Look-Locker inversion recovery (MOLLI) sequence [59]. Native T_1 in the healthy volunteers were aquired with a 5s(3s)3s MOLLI protocol. For further details on imaging parameters see Study I.

One observer acquired native myocardial T_1 values, and blood T_1 and T_1* values from both ventricles. The native myocardial T_1 values were manually acquired by placing a ROI in the septum in a mid-ventricular short-axis T_1 map. In order to avoid partial volume effect from the blood pool the ROIs were conservatively placed in the mid-mural septum. Blood T_1 and T_1* values were acquired with two ROIs in the corresponding T_1 map and T_1* map. Care was taken to avoid including papillary muscle and trabeculae (Figure 5.2). Mean blood T_1 and T_1* values were calculated and converted to the T_1 relaxation rate (R1=1/T_1), resulting in mean blood R1 and R1* values.
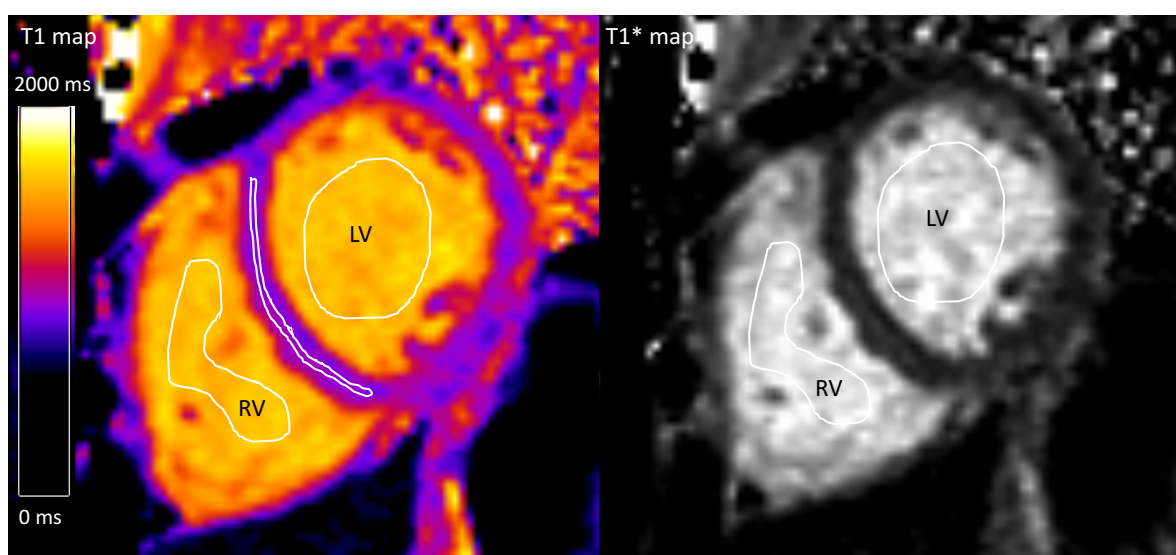
Figure 5.2. The manual delineation of the T_1 and T_1* maps. *This figure displays the regions of interest (ROI) drawn in the respective short-axis maps. The measurements acquired were native myocardial T_1 values, LV blood pool T_1 and T_1* values, and RV blood pool T_1 and T_1* values.*

A linear correlation was assumed and myocardial T_1 values were corrected using the equation:

$$T1corrected = T1uncorrected + constant * (Xmean - Xpatient)$$

where X is the blood measurement of mean R1, mean R1* or hematocrit, mean is the mean for the patient cohort, and the constant was calculated as the slopes from linear regression between myocardial T_1 and the blood measurements.

One observer analyzed the native myocardial T_1 maps acquired in the healthy volunteers. Epi- and endocardial borders were cautiously delineated in the T_1 maps. Global T_1 values were acquired by eroding 10% from each border to acquire the middle 80% of the myocardium. To acquired native T_1 and T_1* blood values, ROIs were placed in both the LV and RV blood pools in both of the respective maps.

5.2.2 Study II

A clinically available free-breathing flow quantification sequence with retrospective ECG gating was used to acquire flow images of the proximal ascending aorta and the proximal main pulmonary artery. For further details on imaging parameters see Study II.

One observer performed flow quantification in the ascending aorta and main pulmonary artery using semi-automated methods with manual adjustment in dedicated software by Vendor 1 and Vendor 2, respectively. ROIs were drawn in the ascending aorta and main pulmonary artery in the magnitude images. These ROIs were automatically outlined in the corresponding phase velocity map. Flow measurements were acquired both uncorrected and with linear background phase correction in Vendor 1, and both uncorrected and corrected with linear and quadratic background phase correction in Vendor 2, respectively. The stationary tissue background correction was performed by maximizing the amount of static tissue. Static tissue was maximized by including as much visual stationary tissue as possible via an increase of the phase deviation threshold. Non-static tissue was excluded by drawing an ROI over the lungs, the heart and the major thoracic vessels (Figure 5.3).
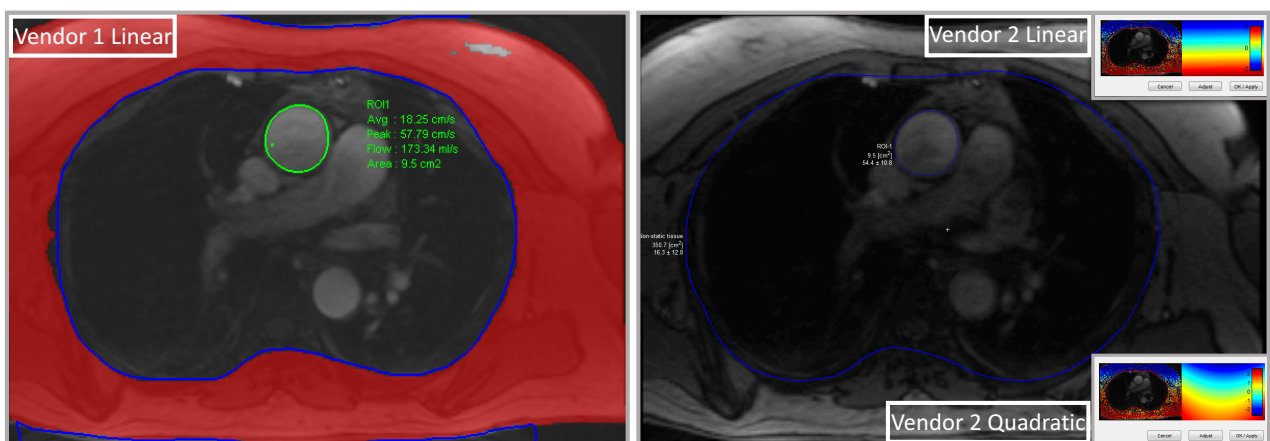
Figure 5.3. Stationary tissue background correction performed in Vendor 1 and Vendor 2. *This image show two identical transverse slices of the thorax which are used for flow quantification in the ascending aorta. The regions of interest (ROIs) in blue shows the excluded non-static tissue. The amount of visual static tissue is seen in red using Vendor 1 (left image). The right image shows Vendor 2. Linear correction is shown in the smaller window in the top right corner, and quadratic correction is shown in the smaller window in the bottom right corner.*

5.2.3 Study III

We acquired one short-axis slice during first pass perfusion imaging, both during adenosine stress (140 microg/kg/min infusion) and at rest. First pass perfusion was performed with the administration of an intravenous contrast agent (0.05 mmol/kg, gadobutrol). The perfusion and MBV maps were generated on the scanner using the Gadgetron inline perfusion mapping software. Figure 5.4 shows a time line over the CMR exam.

Furthermore, we acquired a mid-ventricular native myocardial T_1 map. The map was acquired using a MOLLI sequence [59], with a 5s(3s)3s sampling scheme [25]. We also acquired a mid-ventricular post-contrast T_1 map with the same slice position and sampling scheme as the native T_1 map. This map was acquired following intravenous contrast (total dose over three boluses: 0.2 mmol/kg gadobutrol), both at rest and during adenosine stress (140 microg/kg/min infusion). Using the rest pre- and post-contrast T_1 maps, and stress pre- and post-contrast T_1 maps, respectively we generated rest and stress ECV maps offline. See Study III for further greater detail of imaging parameters.
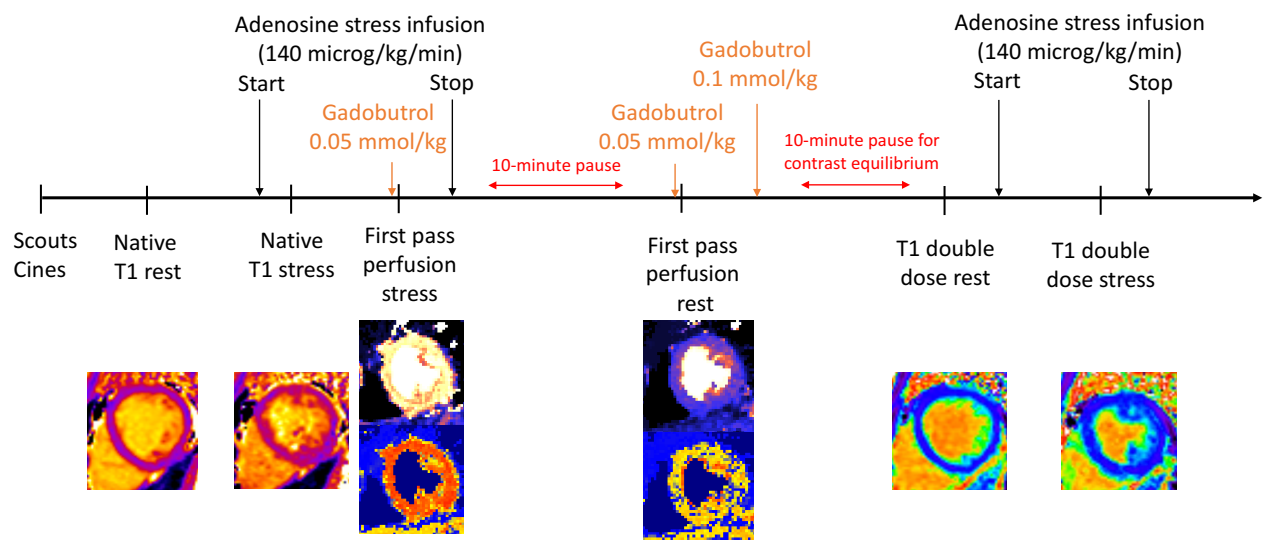
Figure 5.4. Timeline over CMR scan. *Scouts and cines were acquired first, followed by native T_1 mapping a rest. Following 3 minutes of adenosine infusion, native T_1 mapping was acquired, followed by first pass perfusion imaging using gadobutrol (0.05 mmol/kg). After the adenosine infusion was terminated a 10-minute pause followed to reach contrast equilibrium. First pass perfusion images were acquired using gadobutrol (0.05 mmol/kg) at rest and an*

additional dose of gadobutrol (0.1 mmol/kg) was administered. A post-contrast T_1 map was acquired at rest, and at stress following 3 minutes of adenosine infusion.

One observer acquired perfusion, MBV and ECV values by drawing a circumferential ROI in the mid-mural myocardium in the respective mid-ventricular short-axis maps, both at rest and stress.

5.2.4 Study IV

LGE images, and post-contrast T_1 were acquired around 10-15 minutes and 20-25 minutes respectively, after intravenous administration of 0.2 mmol/kg body weight of gadoteric acid (Gd-DOTA). The post contrast T_1 maps were acquired using MOLLI with a 4(1)3(1)2 sampling scheme [118] and motion correction [59]. SynLGE images were generated offline from acquired post contrast T_1 maps using dedicated in-house developed software. Please see study IV for further detail on imaging parameters.

LGE and SynLGE images were anonymized and presented to two independent observers in a random order. The two observers were blinded to patient identity, clinical data and CMR date. The LGE and SynLGE images were evaluated with regards to the presence or absence of ischemic or non-ischemic focal fibrosis. Identification of focal fibrosis in either LGE or SynLGE images required confirmation in two continuous or orthogonal slices.

The cases of disagreement between the observers were re-evaluated together in order to reach consensus. Blinded comparison of the consensus assessment of SynLGE and LGE images was performed for evaluation of the localization and origin of focal myocardial fibrosis on a per-patient basis.

5.3 STATISTICAL ANALYSIS

Statistical analysis was performed using Microsoft Excel (Microsoft, Redmond, Washington, USA) and IBM SPSS Statistics for Macintosh, version 22 and 23 (IBM Corp, Armonk, N.Y, USA). Continuous, normally distributed variables as determined by the Kolmogorov-Smirnov test were reported as mean ± standard deviation. Continuous, non-normally distributed variables, were reported as median [interquartile range]. Ordinal variables were reported as percentages. Means in normally distributed data were compared by the paired or unpaired t-test as appropriate, and standard deviations by the F-test. Medians in non-normally distributed data were compared using the Mann-Whitney U-test or Wilcoxon signed rank test as appropriate, and variability by non-parametric Levene's test. Ordinal variables were evaluated for differences with McNemar's test. Relationships between two continuous variables were assessed with Pearson's linear correlation, and presented as R^2. Multivariate linear regression was performed to obtain slopes for combinations of variables. Statistical significance was defined as $p<0.05$.

5.3.1 Study II

Patient characteristics were dichotomized according to high and low values in relation to the median, and assessed for changes in precision following background correction. Intra-

observer variability was calculated as the difference between two measurements divided by their mean, both for uncorrected and corrected measurements. Change in flow following background correction was calculated as the difference between corrected and uncorrected measurement divided by their mean. Bonferroni correction was applied where *m*=20 and *alpha*=0.05, resulting in *p*<0.0025 as the level of statistical significance for analyses of multiple patient characteristics.

5.3.2 Study IV

Chi square (χ^2) test was used for comparing nominal variables. Cohen's kappa (κ) coefficient was used to evaluate inter-observer agreement and comparing LGE and SynLGE. The κ statistic was interpreted according to the definitions of Landis and Koch where <0.2 indicate poor agreement, 0.2-0.4 fair, 0.41-0.6 moderate, 0.61-0.8 substantial, and 0.81-1.0 almost perfect agreement. With LGE as the reference standard, sensitivity, specificity, NPV and PPV of SynLGE were calculated to detect ischemic and non-ischemic myocardial scar at the segmental level.

6 RESULTS

6.1 DIAGNOSTIC PRECISION

Blood correction for native myocardial T_1 values increased precision with 14% in the derivation cohort, which was maintained with a 13% increase in the validation cohort (Figure 6.1).
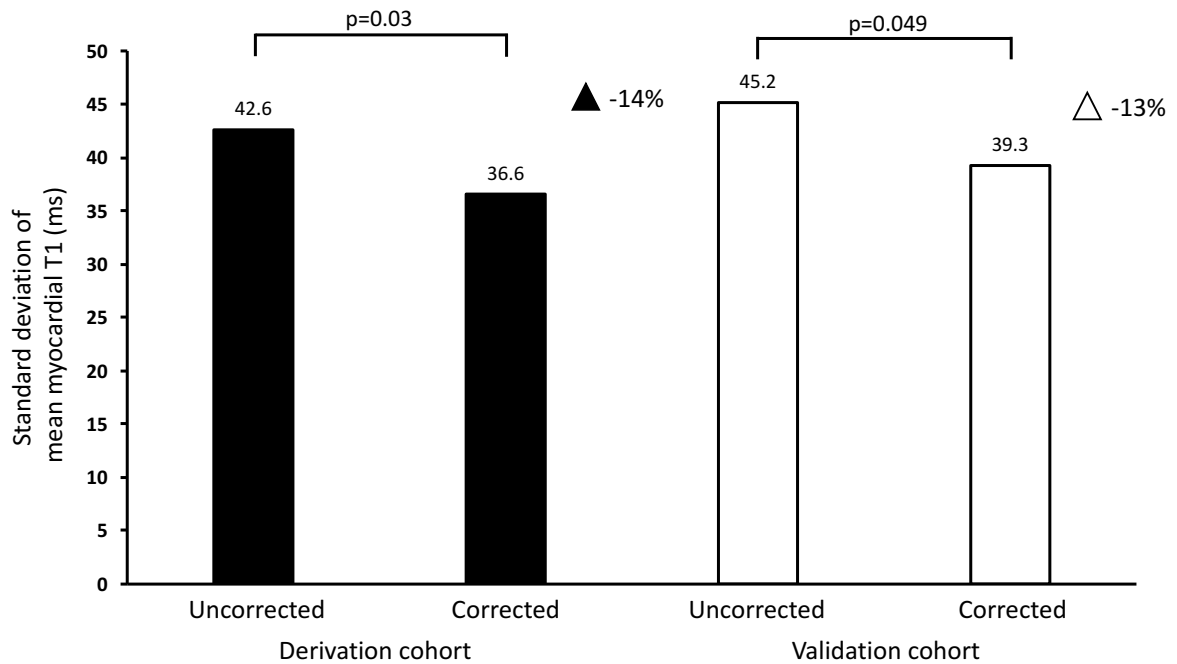
Figure 6.1. Standard deviations of uncorrected and corrected myocardial T_1. *This bar graph shows the standard deviation of native myocardial T_1 (ms) before and after blood correction. The derivation cohort is shown with black bars, and the validation cohort is shown in white bars. The increase in precision in percent is denoted by the triangles.*

The number of patients with a Qp/Qs outside of the normal range decreased following stationary background correction from 16/91 (18%), to 9/91 (10%, $p<0.001$) with Vendor 1 and linear correction, to 9/91 (10%, $p<0.001$) with Vendor 2 and linear correction, and to 6/91 (7%, $p<0.001$) with Vendor 2 and quadratic correction (Figure 6.2).
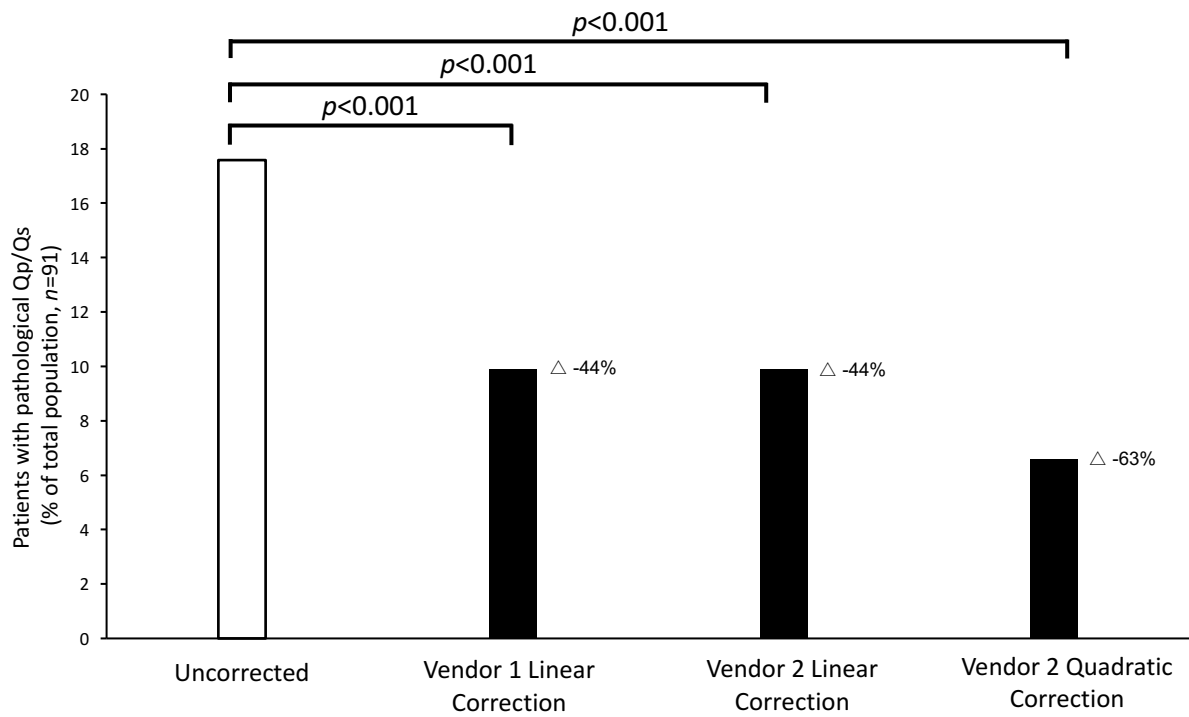
Figure 6.2. Change in number of patients with pathological Qp/Qs following stationary tissue background correction (*n*=91). *Stationary tissue background correction reduced the number of patients with a Qp/Qs outside of the normal range. The triangles denote the reduction of patients with Qp/Qs outside of the normal range in percent.*

Stationary tissue correction increased precision in Qp/Qs compared to uncorrected measurements with 25-30% (Figure 6.3).
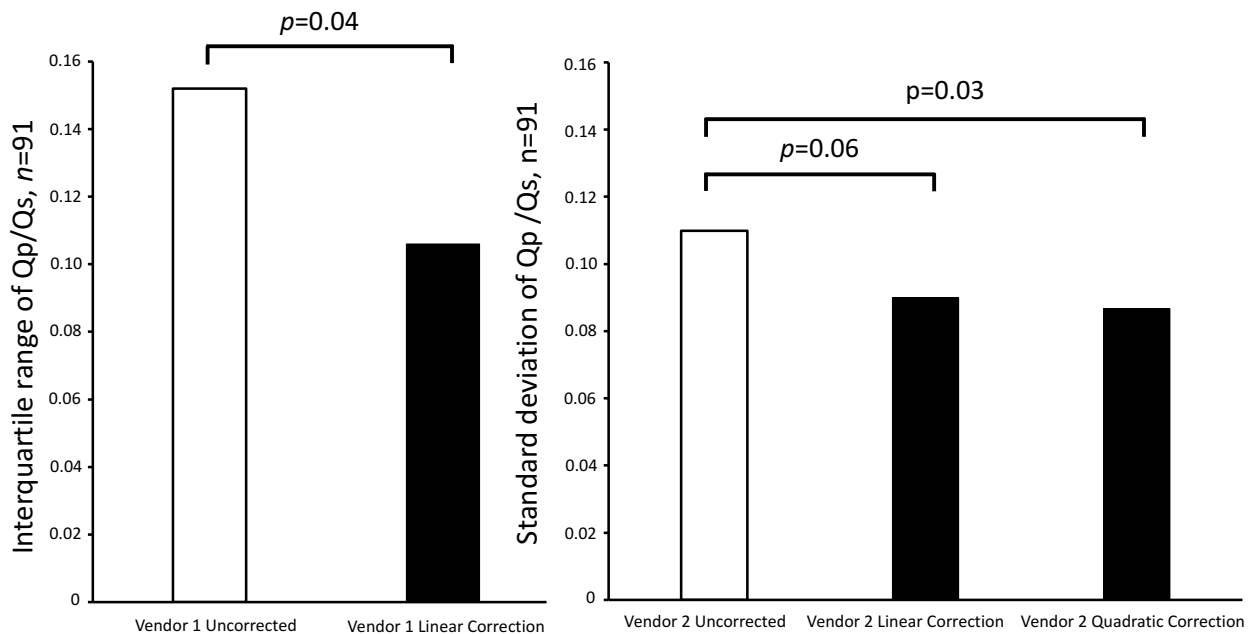

Figure 6.3. The change in precision following linear and quadratic correction with Vendor 1 and Vendor 2 in all patients (*n*=91). *Using linear correction in Vendor 1, the*

precision in Qp/Qs increased. There was a trend towards increased precision in Qp/Qs using linear correction Vendor 2, and quadratic correction increased the precision in Qp/Qs in Vendor 2.

6.2 SEX DIFFERENCES

Blood correction eliminated sex differences in myocardial T_1 values in the derivation cohort (Figure 6.4) and in healthy volunteers (Figure 6.5) and reduced the sex differences in the validation cohort (Figure 6.6)
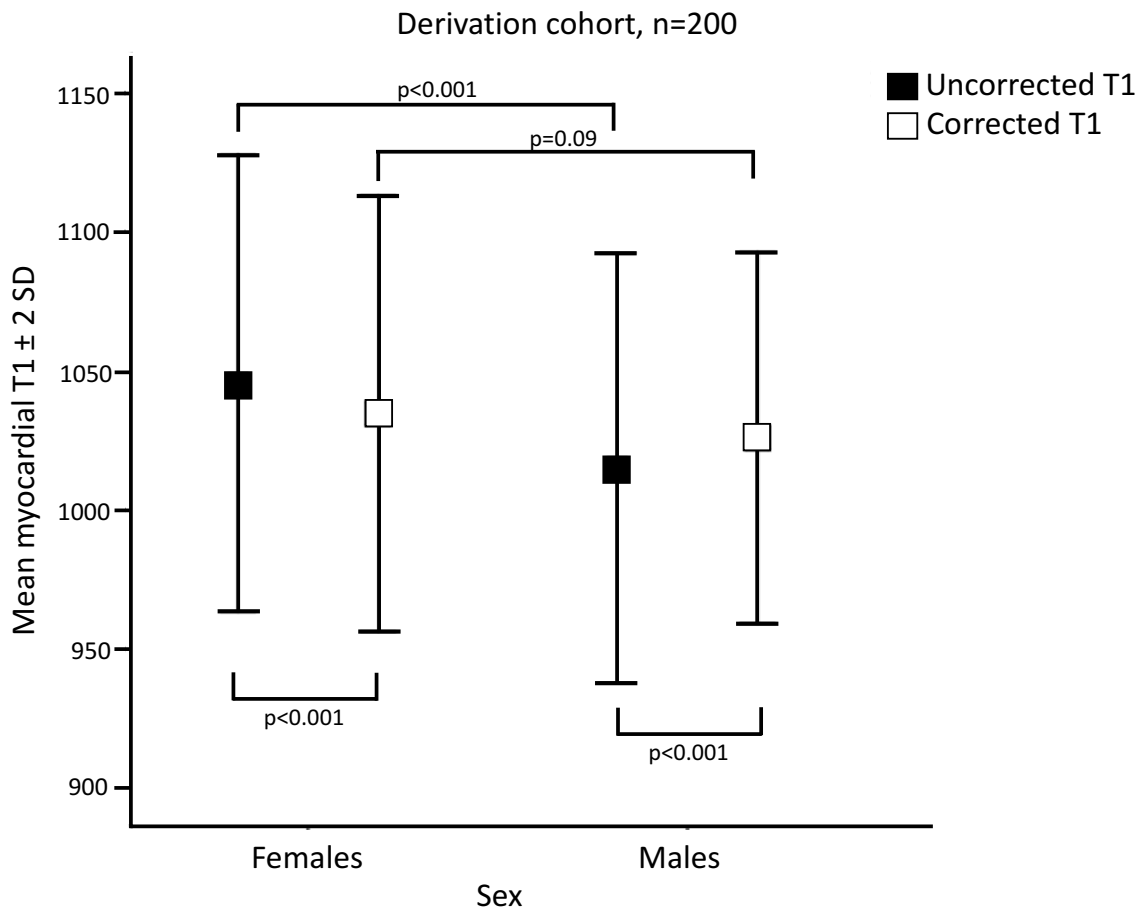
Figure 6.4. Myocardial T_1 values in the derivation cohort separated by sex. *This figure shows the mean±95% limits of agreement before (black boxes) and after (white boxes) blood correction, separated by sex. There was a difference between males and females in the average myocardial T_1 values before blood correction, however that difference was eliminated following blood correction.*
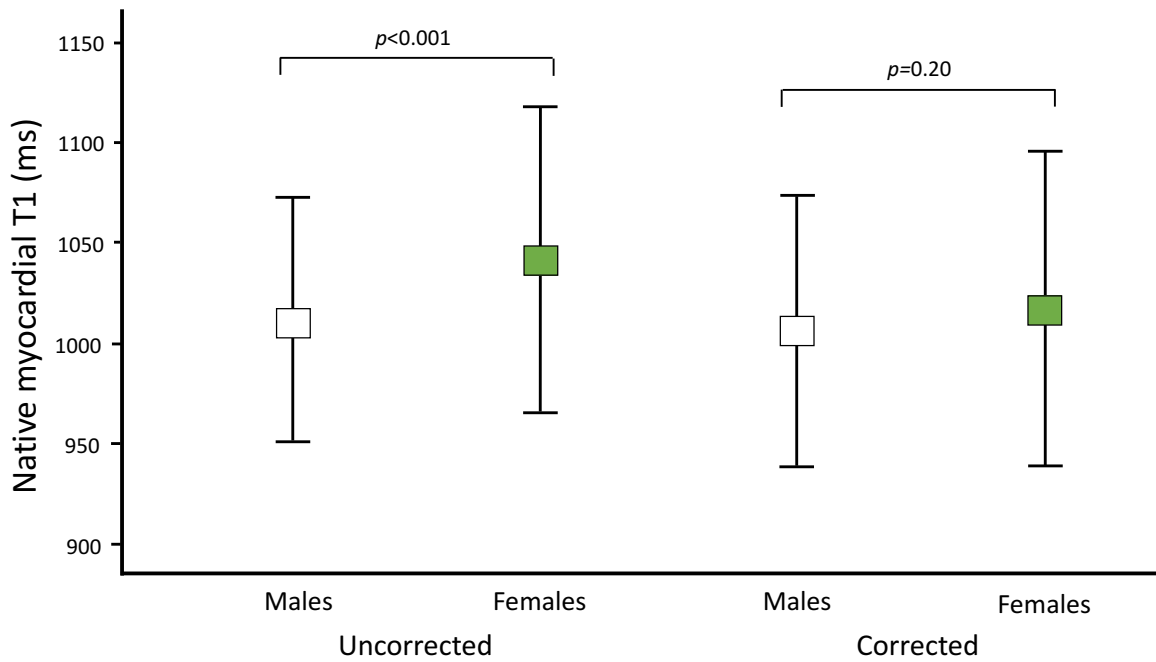
Figure 6.5. Myocardial T_1 values in healthy volunteers separated by sex. *The figure shows the mean±95% limits of agreement for myocardial T_1 values for females (green boxes) and males (white boxes), both uncorrected and blood corrected. The average myocardial T_1 values differed between the males and the females before blood correction, but the difference was eliminated following blood correction.*
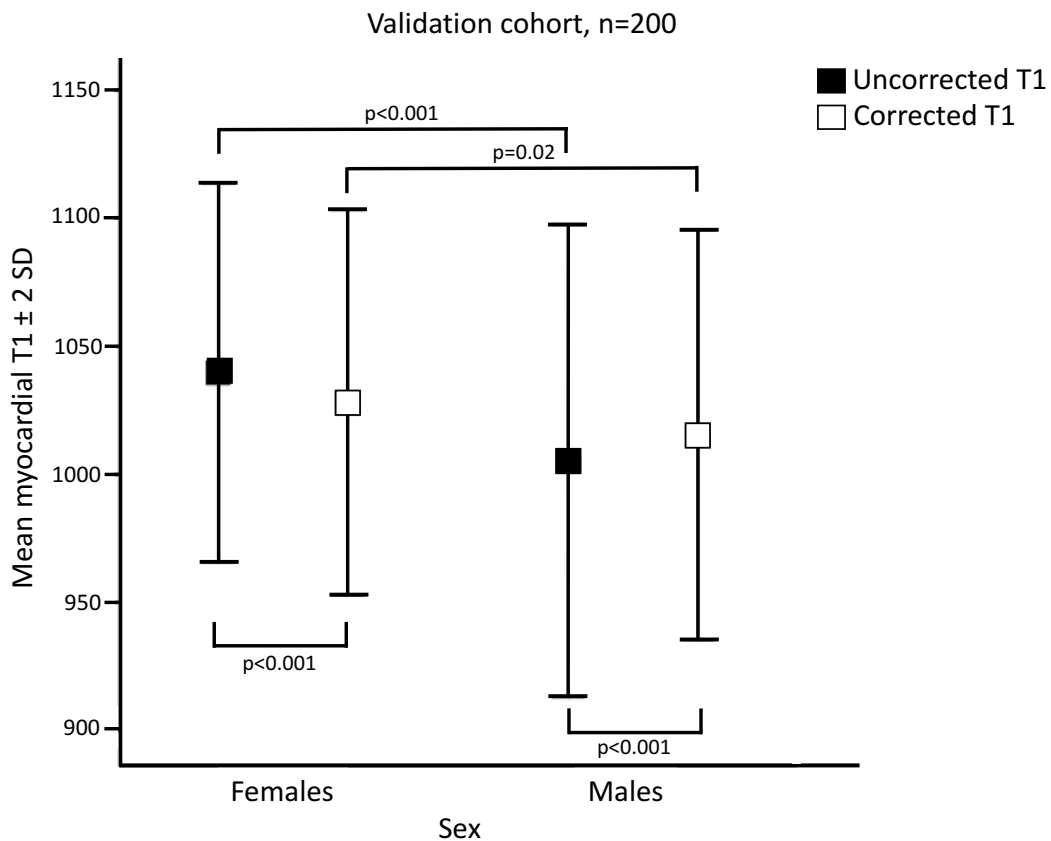
Figure 6.6. Myocardial T_1 values in the validation cohort separated by sex. *This figure shows the mean±95% limits of agreement before (black boxes) and after (white boxes) blood correction, separated by sex. There was a difference between males and females in the average myocardial T_1 values before blood correction. This difference was reduced, but not eliminated after blood correction.*

In females, linear stationary tissue background correction increased the magnitude of Qp/Qs whereas quadratic correction did not (Figure 6.7). However, neither linear nor quadratic correction affected the precision of Qp/Qs. In contrast, linear stationary tissue background correction increased the precision in males using Vendor 1, and did not affect the magnitude (Figure 6.8).
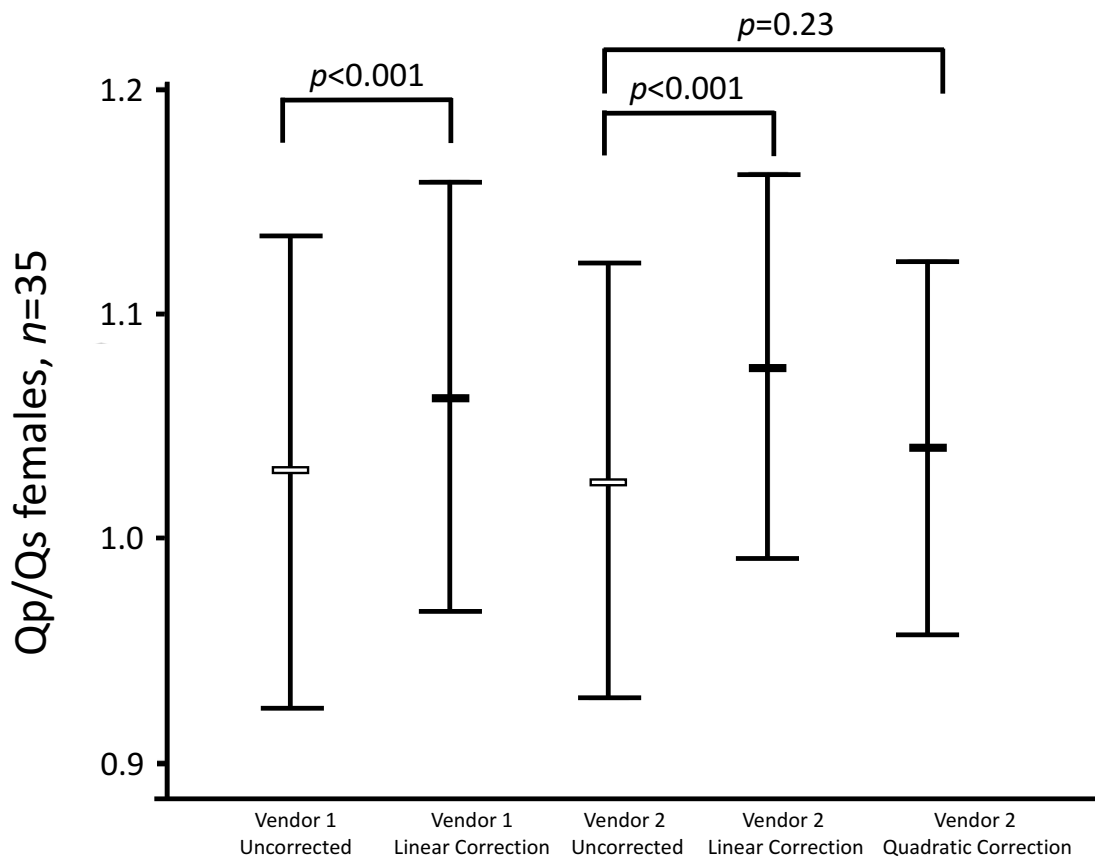
Figure 6.7. Change in mean values for all females following stationary tissue background correction (*n*=35). *The magnitude of Qp/Qs was higher following linear correction in both Vendor 1 and 2, however the magnitude remained unchanged following quadratic correction using Vendor 2.*
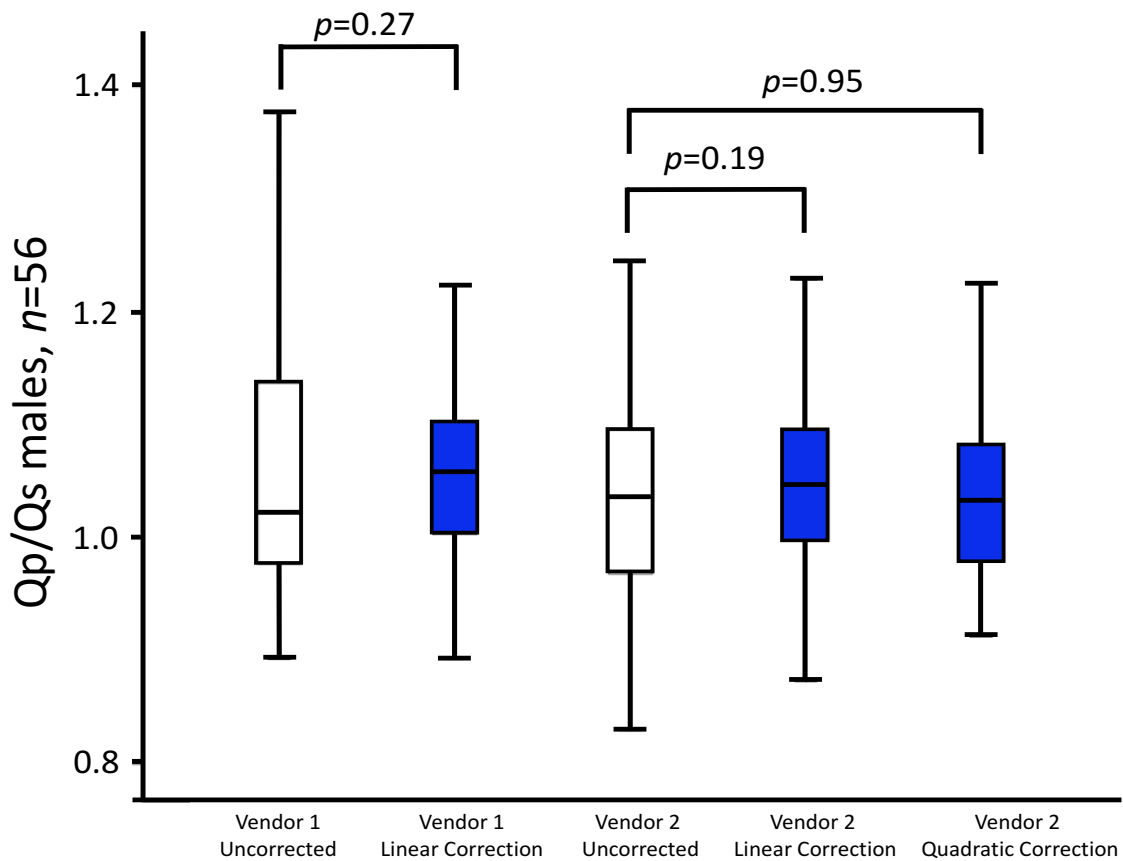
Figure 6.8. Change in median values for all males following stationary tissue background correction (*n*=56). *Neither liner nor quadratic correction changed the magnitude of Qp/Qs in males.*

Healthy female volunteers had higher myocardial perfusion, MBV and myocardial extracellular volume compared to males, both at rest and during adenosine stress (Figures 6.9-11).
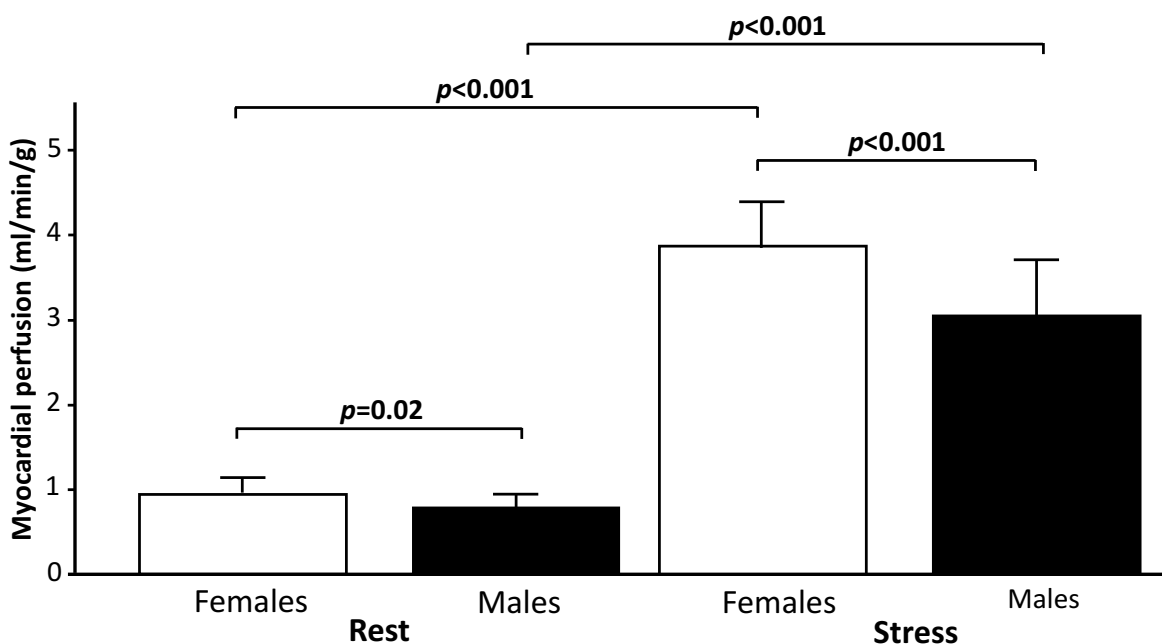
Figure 6.9. Sex differences in myocardial perfusion at rest and during stress. *Females (white bars) had higher perfusion compared to males (black bars) both at rest and during adenosine stress. Error bars show one standard deviation.*
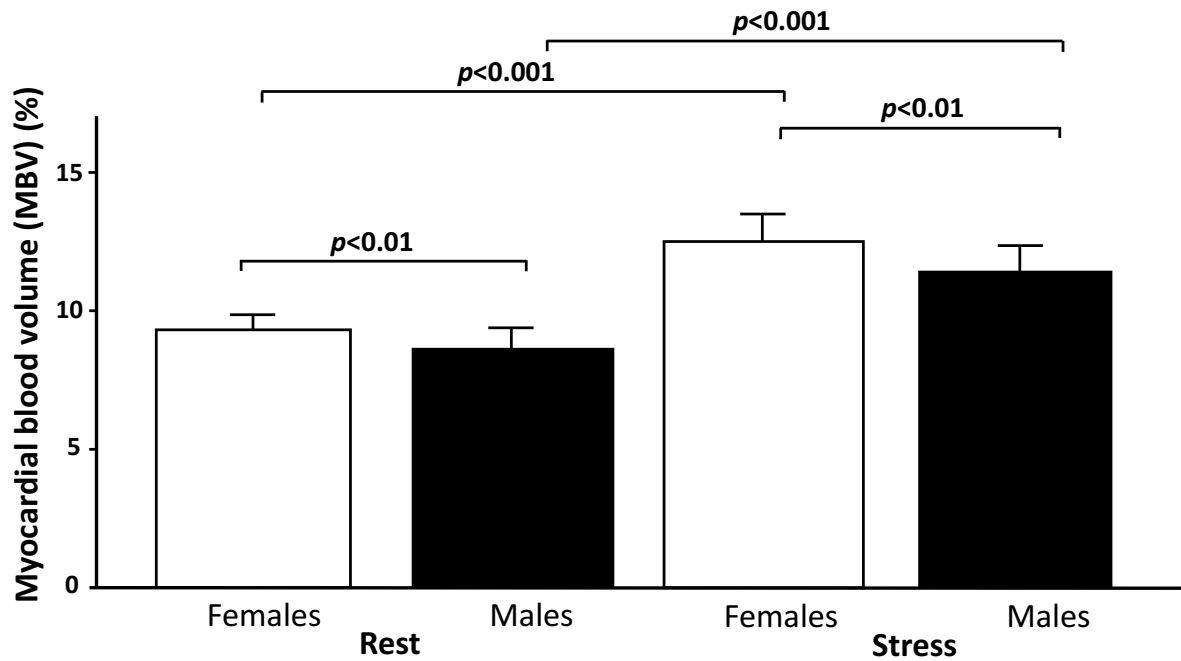
Figure 6.10. Sex differences in myocardial blood volume at rest and during stress. *Females (white bars) had higher blood volume compared to males (black bars) both at rest and during adenosine stress. Error bars show one standard deviation.*
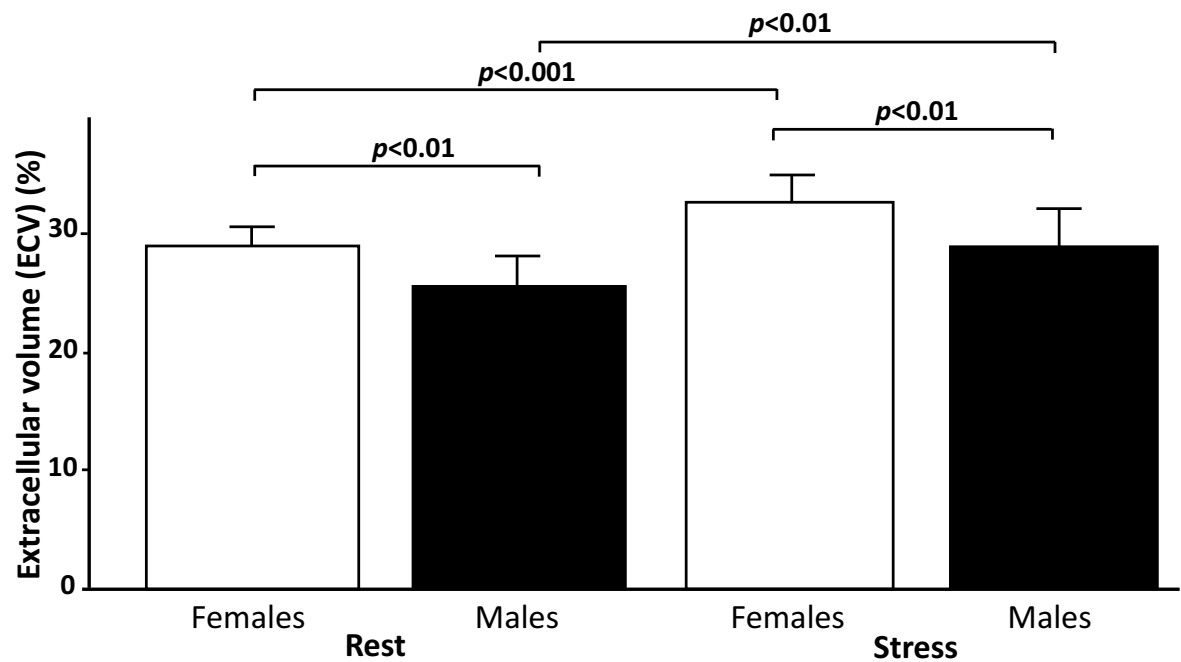
Figure 6.11. Sex differences in myocardial extracellular volume at rest and during stress. *Females (white bars) had higher extracellular volume compared to males (black bars) both rest and during adenosine stress. Error bars show one standard deviation.*

6.3 DIAGNOSTIC ACCURACY

Focal myocardial fibrosis was identified by consensus assessment with LGE in 40% of patients. The patterns of focal myocardial fibrosis were non-ischemic origin (n=24), ischemic origin (n=18) or both (n=3). SynLGE yielded a modest diagnostic sensitivity (77%), a very high specificity (98%), a very high PPV (97%), a high NPV (86%) and an overall accuracy of 98/109 (90%), compared to LGE as a reference standard, Table 2. The overall blinded comparison of SynLGE versus LGE yielded κ=0.78.
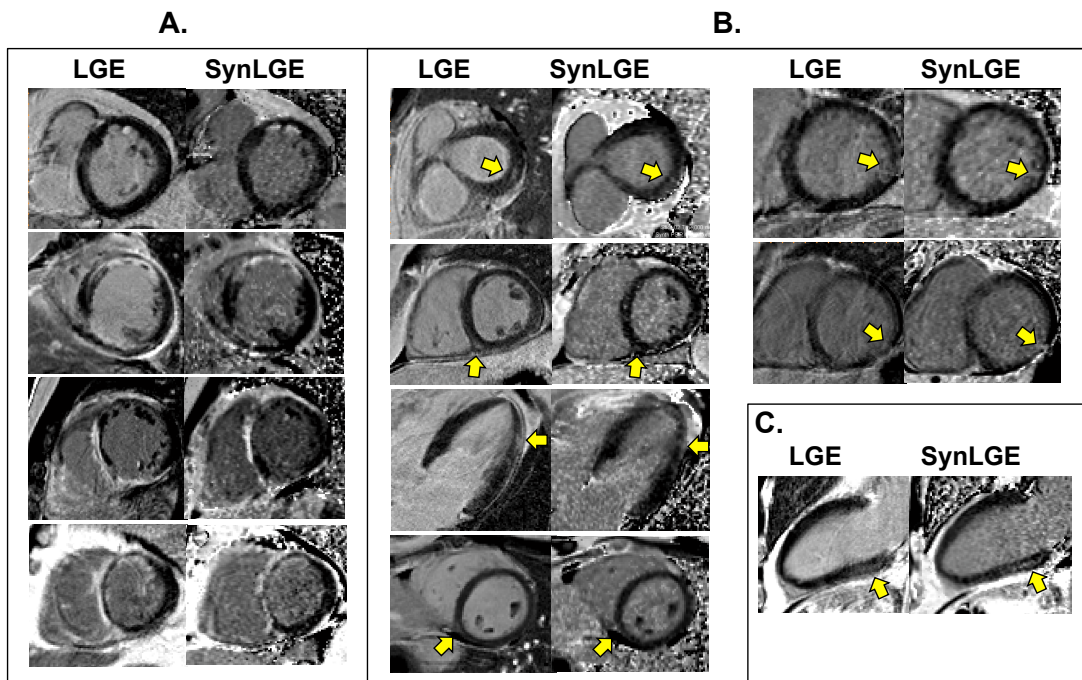
Figure 6.12. *Comparison of late gadolinium enhancement (LGE) images and synthetic LGE images derived from post-contrast T_1 mapping.*
(A) cases with concordant assessment of focal myocardial fibrosis, (B) cases where LGE but not SynLGE detected focal myocardial fibrosis by blinded assessment and (C) focal myocardial fibrosis identified by SynLGE but missed by LGE.

When analyzing ischemic cases, focal myocardial fibrosis was identified in 17% of patients. Compared to LGE, SynLGE yielded a modest sensitivity (83%), a very high specificity (100%), a very high PPV (100%), a very high NPV (96%) and an overall accuracy of 79/82 (96%), Table 2.

When analyzing non-ischemic cases, focal myocardial fibrosis was identified in 22% of patients. Compared to LGE, SynLGE yielded a modest sensitivity (71%), a very high specificity (98%), a high PPV (94%), a high NPV (90%) and an overall accuracy of 81/89 (91%), Table 2.

Table 2. Cases with focal myocardial fibrosis using LGE and SynLGE

a) Overall	LGE		
SynLGE	**Positive**	**Negative**	**Total**
Positive	34	1	35
Negative	10	64	74
Total	44	65	109

b) Ischemic	LGE		
SynLGE	Positive	Negative	Total
Positive	15	0	15
Negative	3	64	67
Total	18	64	82

c) Non-ischemic	LGE		
SynLGE	Positive	Negative	Total
Positive	17	1	18
Negative	7	64	71
Total	24	65	89

a) Shows the overall analysis for SynLGE versus LGE as a reference standard (n=109 patients). Chi square p<0.0001 b) Shows the analysis for ischemic focal fibrosis (n=82 patients). In this analysis, the patients (n=3) with both ischemic and non-ischemic focal fibrosis were excluded. c) Shows the analysis for non-ischemic focal fibrosis (n=89 patients). In this analysis, the patients (n=3) with both ischemic and non-ischemic focal fibrosis were excluded.

Abbreviations: LGE = late gadolinium enhancement; SynLGE = synthetic LGE.

7 DISCUSSION

We have identified sex differences in several aspects of clinical CMR imaging that affect precision, and have explored post-processing methods for increasing diagnostic precision and accuracy in clinical CMR. Furthermore, we have provided mechanistic insights into the normal myocardial physiology by exploring different parameters of the myocardial circulation during rest and stress in healthy volunteers. It is evident that post-processing is a powerful tool to increase diagnostic precision, however in a clinical setting post-processing poses a tedious time challenge and it would therefore be beneficial with increased precision in the imaging sequences.

7.1 DIAGNOSTIC PRECISION IN NATIVE T_1 MAPPING

We have proposed and validated a blood correction method for clinical native T_1 mapping using the 5(3)3 MOLLI protocol with the mean (average LV + RV) blood measurements. Using the mean blood measurements allows for automated blood correction T_1 maps to be produced, by automated blood pool detection. Further studies are needed where native T_1 maps and blood corrected T_1 maps are compared head to head, in order to see how blood corrected T_1 maps perform with native T_1 maps as an independent reference standard. It has been suggested that blood correction may increase precision in detection of fibrosis in the LV in patients with pulmonary hypertension [119]. It would be interesting to see if this could be applicable to diseases that are detected by native T_1 mapping, such as iron-overload cardiomyopathy, Anderson-Fabry disease or amyloidosis. The accuracy and precision could likely increase in two ways – either by reducing the reference values and thereby values that are considered normal today would be considered diseased, or by blood correction pushing the T_1 values outside the normal range on a per patient basis.

Anderson-Fabry disease is characterized by accumulation of glycosphingolipids in the cardiomyocytes, which lead to a decrease in native T_1 values [120]. Imagine a woman with Anderson-Fabry disease and let's say that her hematocrit is in the lower range. Her blood has a lot of plasma with high T_1 and less hemoglobin with low T_1, so her mean native blood T_1 is 1673 ms and her myocardial native T_1 is 903 ms, just above the lower limit of normal of 900 ms. By applying our validated blood correction model on a per patient basis, her native T_1 value becomes 890 ms – clearly diseased. However, by adjusting the reference values 900 – 1100 ms with a 13% reduction, assuming that the reduction is equally distributed, the reference values would be 913 – 1087 ms, thus making 903 ms diseased too. One might speculate that blood corrected native T_1 maps can add benefit in difficult cases like this, likely as an effect on both the changes in native T_1 in a per patient basis and in the reduction in the normal ranges. The accuracy and precision of native T_1 maps are, by definition, going to increase as a result of the reduction in normal ranges with blood corrected native T_1 maps. It may be that the changes on a per patient basis will add to the accuracy and precision of blood corrected T_1 maps, by further separating normal from diseased values as exemplified with the woman with Fabry's disease. With a native myocardial T_1 value of 890 ms and reference

values of 913 – 1087 ms, it is obvious that this woman has myocardial engagement of Fabry's disease. However, blood corrected T_1 maps need to be studied compared to native T_1 maps, and compared to outcome during follow up.

7.1.1 Choice of protocol

There are several MOLLI protocols in clinical use for native T_1 mapping, and during the course of this thesis the clinical protocol at our site has changed from 5(3)3, to 5(3s)3 to 5s(3s)3s, which is the protocol shown to have the best precision. Furthermore, the 5s(3s)3s protocol is highly reproducible, has few image artifacts, and requires only a short breath-hold. The ShMOLLI protocol performs very similar to the 5s(3s)3s protocol, however with a 30% loss of precision [25]. The best accuracy is achieved with SASHA, however SASHA suffers from limited precision [58]. Therefore, Saturation-Pulse Prepared Heart-rate independent Inversion-Recovery (SAPPHIRE) was developed [121], which combines the saturation and inversion recovery approaches, thus mitigating heart rate dependency and increasing precision. In head to head comparisons in phantoms, MOLLI and ShMOLLI had higher precision compared to SAPPHIRE and SAHSA, whereas SAPPHIRE and SASHA had higher accuracy compared to MOLLI and ShMOLLI [122]. It is worth noting that the accuracy differed by 63 ms with ShMOLLI, and 44 ms with MOLLI, and that there was a trend towards higher precision with MOLLI compared to ShMOLLI, (4.0 ms compared to 5.6 ms, p=0.07). The higher accuracy in SAPPHIRE and SASHA is due to saturation recovery imaging circumventing several of the issues with inversion recovery such as T2 dependence, magnetization transfer effects, and the dependence of inversion efficiency [25, 58, 122]. Extensive work on increasing the precision of saturation recovery techniques include free-breathing SASHA with a precision similar to breath-held 5(4)3 MOLLI over 30 s sampling [123] [*sic*], and SASHA with less than 30% precision-loss compared to 5(3)3 MOLLI at 3T [124].

7.1.2 The future of T_1 mapping

In the clinic, today one has to choose between precision and accuracy with regards to the choice of IR techniques (MOLLI and ShMOLLI) versus SR techniques (SASHA and SAPPHIRE) for native T1 mapping. MOLLI has better precision, but worse accuracy compared to SR techniques. From a clinical perspective, one might argue that in the clinical context of native T_1 mapping, precision is more important than accuracy. Quantification allows for an objective measure to detect or follow as physiological phenomenon over time, following that the measurements have high precision. Of course, the best-case scenario would be a measurement that is both accurate and precise. However, if forced to choose today between MOLLI and precision or SAHSA and accuracy, the argument for choosing MOLLI over SR techniques would be based on precision. In order to identify subtle changes, low variability is paramount, even if the actual measure may systematically differ from the true value. This is evident with MOLLI in the clinical situation today. The technique is widely available, and is a highly sensitive measure of tissue characterization, which has demonstrated an ability to differentiate disease from healthy myocardium, despite

52

inaccuracies. There is clinical knowledge on what a native T_1 value signifies using a MOLLI sequence, and how it can be used to guide patient management. SR techniques still have the advantage that, with more research, the precision may increase, thus becoming both accurate and precise for measuring T_1. In that case, one could argue that SR techniques have to show an incremental benefit compared to MOLLI to gain acceptance in the field.

Another benefit of SR techniques is that the ECV-measurements seem to be more accurate, compared to MOLLI measurements. Furthermore, SR techniques also seem to have higher accuracy across the LV – same mean value across all three slices compared to MOLLI [124]. ECV has clinical prognostic importance [125], and this could further add to the clinical applicability of SR techniques, despite that they are currently not as commonly used as MOLLI. However, it would be of great importance that SR techniques becomes precise and reproducible, so that the CMR field can reach a consensus on which technique to use in order to allow for multicenter studies, and for T_1 mapping to become a well-established tool for clinical decision-making.

7.2   DIAGNOSTIC PRECISION IN FLOW QUANTIFICATION

We have shown that post-processing by stationary tissue background correction reduces measurement variability in Qp/Qs, and furthermore reduces the number of patients with a Qp/Qs outside of the normal range. The stationary tissue background correction of phase contrast velocity encoded images are integrated in the clinical software products, are used clinically every day and the correction takes little additional time to perform. The differences in precision are relatively small in absolute numbers, but as much as 25-30 % in relative terms. Furthermore, the number of patients with a Qp/Qs outside of the normal range is decreased with over 50% following stationary background correction. This is in stark contrast to previous findings in patients with congenital heart disease without known cardiac shunts, where the number of shunts increased following correction [126]. However, that study was small (*n*=24), and patients with congenital heart disease may have more valvular disease, which may have impacted the results as the effect of valvular disease on stationary tissue background correction has not yet been fully evaluated. The main limitation in our study is the lack of an independent reference method to determine that the patients indeed had no shunt. Future studies could be performed in a clinical population that have been deemed to have no shunt by transesophageal echocardiography. Furthermore, the normal variability of Qp/Qs in unknown, therefore it was not possible to do an *a prior* power and sample size calculation. Moving forward, the results in this study can be used as a basis for either estimation of a plausible change in Qp/Qs values, or calculating a sample size needed for a specific outcome. Furthermore, it would be interesting to see what actually happens in a patient cohort with known cardiac shunts – does the Qp/Qs increase or decrease following stationary tissue background correction? Looking at the results from our cohort without cardiac shunts, stationary tissue background reclassified patients from shunt to no shunt in 10-12 cases. One might hypothesize that Qp/Qs increases following stationary tissue background correction and that, in a few cases, patients would be reclassified from having no

shunt to having a shunt. In summary, our data supports that it is of clinical importance to perform stationary tissue background correction in the clinical setting to reduce variability and increase diagnostic precision.

7.3 ISCHEMIC HEART DISEASE AND CMR

CMR allows for a comprehensive, multi-parametric cardiac assessment, and is rapidly moving towards a becoming a one-stop-shop technique. CMR has superior diagnostic properties in ischemic heart disease, with important prognostic implications [127]. Seven to fifteen percent of ACS patients have non-obstructive coronary arteries [128], and this is more common in women than in men [129]. CMR can identify different underlying etiologies in these patients [130, 131]. Overall, CMR can provide a final diagnosis in the majority of patients, and has a significant clinical impact in two thirds of patients by either providing a new diagnosis or changing clinical management [132]. Furthermore, CMR can guide revascularization in coronary chronic total occlusion to reduce ischemic burden [133]. Since 2013 CMR has a class 1B indication for risk stratifications in patients with stable, obstructive CAD to guide clinical decision making, and assess patients with intermediate PTP of CAD [106]. Stress CMR also has a class 1A indication for assessing residual ischemia and viability in STEMI patients [97], and has been given a class 1A indication for assessing suspected CAD in patients with intermediate PTP for myocardial revascularization [134]. However, as suggested by Study III, there is a current knowledge gap on sex differences in CMR and how these affect diagnostic precision.

7.3.1 Differences between the sexes in ischemic heart disease

Older women have a worse outcome in ACS compared to men, often attributed to that they are older, have more co-morbidities and therefore receive less aggressive treatment. It would therefore be logical to assume that younger women, that do not have more co-morbidities, receive the correct treatment and therefore having a reduced the mortality rate. On the contrary, middle-aged and younger women have a higher risk of adverse events following an AMI. Women that are younger than 55 years old have a three-fold higher mortality rate in hospital and an increased risk with 50% of death over 2 years compared to young men [135-137]. Some data suggest that younger women are sicker on admission and receive less aggressive and effective treatment and care [138-141]. Other explanatory factors are that women present with different symptoms [142] and that young women more often suffer from depression [143]. These factors are more gender-related and this is why it is of such importance to investigate physiological, sex-related factors.

It is evident in Study III that women have higher myocardial perfusion and blood volume compared to men. The healthy volunteers in the study were predominately young, thus providing a potential sex-related factor for the differences in outcomes in younger women. With a higher myocardial perfusion and MBV it is possible that the female myocardium is more susceptible to ischemia, causing more damage in the myocardium in females compared to males when exposed to ischemia. Estrogen has been shown to have a vasodilatory effect

54

[144], and it has been suggested that the loss of estrogen in peri- and postmenopausal women may cause vasoconstriction leading to ischemia with normal coronary arteries [101]. In Study III we also learned that young women have higher ECV compared to men. MBV and ECV are related, and we postulate that the increase in MBV contributes to the increased ECV in women compared to men. This is due to the fact that the technical methodology for ECV mapping utilizes the plasma volume (the extracellular space of the intravascular compartment) to calculate the ECV in myocardium. However, it is also possible that the increased ECV contributes to the increased MBV in women compared to men. Furthermore, all variables that differed between the sexes in Study III were investigated for with regards to linear correlation with MBV, myocardial perfusion and ECV, respectively. No parameter correlated with MBV, myocardial perfusion or ECV at both rest and stress, respectively. This suggests that sex is an important, independent factor that is not explained by factors such as body surface area.

7.3.2 Physiological measurements of myocardial ischemia

In the healthy heart, myocardial perfusion is tightly regulated by dynamic changes in both the epicardial and intramyocardial coronary vasculature, as well as the downstream microcirculation. Roughly 75% of the oxygen is extracted from the coronary circulation by the myocardium during rest. This leaves a minimal oxygen reserve, and therefore, any increase in oxygen consumption requires an increase in myocardial perfusion. The regulation of myocardial perfusion is mainly controlled by the microcirculation, as the epicardial coronaries only contribute with roughly 10% of the coronary resistance. The capillary system and venules serve as capacitance vessels, holding 90% of the intramyocardial blood volume, but offer only minimal resistance. The coronary resistance is primarily controlled by prearterioles and arterioles during normal conditions. As a result of autoregulation, myocardial perfusion remains relatively constant over a wide range of perfusion pressures, through shear stress and pressure-dependent myogenic mechanisms. Coronary flow decreases exponentially below the lower pressure limit of autoregulation, which results in myocardial ischemia. The complexity of the dynamic control of myocardial perfusion further underscores the complex and difficult task to truly identify myocardial ischemia, both invasively and non-invasively.

7.3.2.1 *CFR, RFR, FFR and hyperemic myocardial perfusion*

CFR is determined by the maximal hyperemic perfusion divided by the baseline perfusion. CFR will be affected both by epicardial stenosis, and microvascular disease, and normal ranges depend of method of quantification, however CFR <2.0 is generally considered to be consistent with ischemia [145]. A closely related parameter is relative CFR (RFR), which can be used to assess an epicardial stenosis. RFR is defined by dividing the maximum stress perfusion in a diseased coronary segment by the maximum stress perfusion in a segment without disease [146, 147]. In the situation where microvascular disease is not present, the RFR for a stenosis should be identical to the pressure-derived fractional flow reserve (FFR), however RFR as a measurement does not capture microvascular dysfunction like CFR [146].

Hyperemic myocardial perfusion (ml/min/g), sometimes referred to as hyperemic MBF, has also been suggested as a measurement for detecting ischemia by using a threshold during hyperemia [148]. All of these non-invasive measurements can now be measured with quantitative CMR perfusion mapping. However, as shown in Study III, sex differences might have to be accounted for, especially in young people. This is particularly important when using myocardial perfusion as a parameter, as sex-dependent cut off values for ischemia might be necessary. Currently, we are lacking knowledge on sex differences in myocardial perfusion using CMR in other age groups, as Study III was conducted in primarily in young volunteers. Drawing upon the results from heart rate variability studies on sex differences [85], it is possible that sex differences decrease after 50 years of age (likely due to menopause). In a cohort without obstructive CAD, there was a clear sex difference in myocardial perfusion using PET, both at rest and during stress, which was still evident following correction for rate pressure product (RPP), which is a marker of cardiac work [149]. However, there was no sex difference in CFR, which is logical since myocardial perfusion is higher during both rest and stress, and this effect is accounted for by the ratio between them. This supports that, when using myocardial perfusion for ischemia detection, it is likely important to take sex differences into account.

FFR is an invasive measurement where the change in pressure over a stenosis is measured, during maximal hyperemia. FFR is based on the notion that pressure varies linearly with flow, so a drop in pressure reflects a drop in flow over a stenosis, and thereby identifies ischemia. FFR has emerged as the reference standard to evaluate stenosis severity and guide treatment [150-152]. There are several different methodological issues with all of these parameters, and furthermore, there are complex relationships between diffuse microvascular dysfunction and focal obstructive CAD.

7.3.2.2   *Ischemia as a physiological continuum of focal and diffuse disease*

All of the above-mentioned measurements aim to, in a binary fashion, separate healthy from disease, or significant from non-significant myocardial ischemia. This reflects the clinical ideal: a clinician desires a simple cut-off to perform an intervention with known effects on hard endpoints like mortality. However, excepting that one single measurement can dichotomize the complex reality of myocardial ischemia in all patients with different diseases, backgrounds, ethnicity and sex is likely an oversimplification [153], and likely underestimates the complexity of the myocardial microcirculation. Van Horssen *et al.,* has shown that epicardial penetrating arteries define separate perfusion territories, that likely relate to borders of ischemic and infarcted tissue in dogs [154]. The perfusion territories increase in size, but decrease in number when moving from the epicardium towards the endocardium, highlighting that the endocardium is only perfused by a small subset of penetrating arteries. As the evolution of infarcts in dogs is most similar to humans compared to other species [155], it is possible that the microcirculation is similar in humans. This could add to the knowledge of the pathophysiology of INOCA: if microvascular disease, or only mild stenosis, develops in the few penetrating arteries, the endocardium may be highly

susceptible to the emerging ischemia, compared to the epicardium that has more vessels with smaller perfusion territories. It would be interesting to see if there are sex differences in the coronary microvasculature. Larger and fewer perfusion territories could be an explanatory variable for the sex differences in MBV.

There are different causes myocardial ischemia: the focal epicardial coronary stenosis, the diffuse INOCA due to microvascular disease and the combinations of the focal and diffuse disease of different severity. It is clear that CFR, RFR, FFR and myocardial perfusion all can identify severe stenosis in need of revascularization [146, 153, 156]. However, it is likely only CFR that can identity diffuse microvascular disease, INCOA, and also has the advantage of identifying both flow-limiting stenosis and microvascular disease [157]. In case CFR is used, the data suggests that there is no need for sex specific cut-off values. Focal stenosis is associated with diffuse disease [158], which has the implication that the risk with the focal disease needs to be higher than the risk with the diffuse disease in order for intervention to be successful. Furthermore, an FFR can be low in a visually small stenosis [159], but with a normal CFR, and it is unclear if these patients will benefit from revascularization. An FFR can also be high, but with a low CFR, thus reflecting diffuse microvascular disease. FFR after intervention inversely correlates with risk, which is likely a reflection of residual diffuse microvascular disease [158]. FFR thereby fails to identify these patients, however they can likely be identified by CFR or myocardial perfusion. However, MBV has also become an interesting parameter to assess myocardial ischemia. In case of a significant stenosis, the vasculature would be fully dilated at rest and during stress there is no reserve left to dilate. This means that the MBV is high a rest, with little to no response during stress in obstructive CAD. Further studies on MBV maps in patients may elucidate this further, and highlight if sex difference exist in patients with obstructive CAD.

Significant stenosis can be detected with the response native T_1 values during stress [160]. Furthermore, the response in native T_1 values shows promise in differentiating between obstructive CAD and microvascular disease [161]. As the cut-off value was a ratio of native T_1 native values between rest and stress, sex differences in native T_1 is likely mitigated. However, this needs to be investigated to ensure that sex differences in the ratio of native T_1 values at rest and stress does not affect the diagnostic ability.

7.3.2.3   Integrating all physiological parameters

There has been a remarkable evolution in cardiology for guiding the treatment of stable obstructive coronary artery disease, moving from anatomical to physiological measurements propelled by paradigm-shifting introduction of FFR [152]. However, it is evident that the binary decision of intervention is not sufficiently answered by one dichotomous parameter. As suggested by Gould and Johnson [153], the field needs to continue the journey towards handling the coronary circulation as a complex and multidimensional system, that requires an integration of several variables to make the decision to do an intervention or not to an intervention. With the findings of sex differences of several different parameters pertaining to the coronary circulation, one might argue that it is not just the different measurements of the

coronary circulation that need to be taken into account, but also sex. It is evident in normal myocardial physiology that sex is a relevant parameter and should be considered, as women have higher myocardial perfusion, MBV and ECV compared to men. The medical field is moving towards personalized medicine – and therefore one might argue that the imaging field needs to consider personalized diagnostics, the choice of imaging method should also be based on several parameters such as age, sex, ethnicity in order to increase diagnostic precision and accuracy.

7.3.3   CMR compared to other imaging modalities

Previously, myocardial ischemia has been detected by CMR using qualitative assessments, or semi-quantitative assessments based on the time-intensity curves following first pass perfusion with a gadolinium-based contrast agent. With the recent development of quantitative perfusion mapping [45] evaluated in this thesis, CMR now has the same ability as PET to quantify of both CFR and visualization of single vessel stenosis [162]. Myocardial contrast echocardiography (MCE) has been validated for absolute quantification of MBV and myocardial perfusion [163, 164]. MCE utilizes a continuous infusion of microbubbles as a contrast agent which are destroyed by a high-intensity acoustic signal, and the inflow of microbubbles thereafter generates time-acoustic intensity curves. The main disadvantages of MCE are operator dependency and limited spatial resolution due to the acoustic window. SPECT utilizes the relative intensity of radiotracers to identify areas with reduced myocardial perfusion, and thereby inherent lacks the ability of absolute quantification of myocardial perfusion, and detection of INOCA.

A reason for the limited sensitivity and specificity of some imaging modalities, particularly in women, may be the overrepresentation of INOCA in women. Historically, imaging modalities haven been validated for identifying stable obstructive CAD against anatomical assessment with angiography. With the emerging knowledge on physiological measurements for intervention in obstructive CAD, and the knowledge on INOCA there is a need to reevaluate the different imaging modalities with regards to their potential to identify stable coronary syndromes; obstructive CAD and INOCA, and further characterize the INOCA subgroup with myocardial ischemia.

7.3.4   Imaging of focal fibrosis with CMR

The presence of ischemic heart disease can be detected by LGE, and LGE is the references standard for viability assessment [10]. We showed that SynLGE had limited sensitivity to detect focal myocardial fibrosis, commonly referred to as scar, of any origin compared to LGE. However, SynLGE has been shown to have an excellent agreement with LGE in ischemic heart disease [165, 166]. In our study, we looked at both ischemic and non-ischemic focal fibrosis, which may account for some of the differences in result. Furthermore, only SynLGE and LGE images were assessed in this study. In order to evaluate how SynLGE performs clinically, a study could be designed in a way where the observers perform a full clinical evaluation, with both native T1 maps, cine images and ECV maps. However, one of

the observers may only use SynLGE images, and the another only LGE images. The endpoint would be presence of focal fibrosis of any origin on a per patient basis, with LGE as the reference standard. This would reflect the clinical decision-making, where images of focal fibrosis constitute one piece of the puzzle.

Clinically one may come across the issue of scarring or focal myocardial fibrosis that heals, and becomes no scarring, especially in non-ischemic etiology. There has been a shift towards calling the non-ischemic LGE for inflammation instead of scarring, however LGE can be present without increased native T_1. Drawing upon *rubor, tumor, calor* and *dolor,* the classic signs of inflammation that Roman scholar Celsus defined in the first century A.D., one would expect native T_1 to be increased and reflect edema in case we have inflammation. The most common is of course that LGE and increased native T_1 are present simultaneously, and as the edema decreased, LGE either heals or leaves a permanent scar. This would be very interesting to investigate further, what is actually causing the focal LGE in the non-ischemic etiologies that with times heals without leaving a scar.

7.4   THE FUTURE FOR QUANTITATIVE CMR

CMR is an important tool in clinical cardiology where the relatively high spatial resolution allows for the assessment of both LV function and mass, the tissue characterization allows for the evaluation of the presence and origin of focal fibrosis, edema, and i.e. iron, and with the quantitative perfusion mapping both obstructive CAD and INOCA can be quantified. CMR has evolved to a one-stop-shop, an imaging tool where almost any cardiac question can be answered. The CMR field has to reach a consensus on which method to use for T_1 mapping, work on even more rapid imaging for i.e. valvular imaging to contribute to flow quantification and gain clinical knowledge in quantitative perfusion mapping to even further distinguish CMR from other imaging methods. CMR will always have the advantage of being free from ionizing radiation, and inherent high signal contrast. Furthermore, new applications of non-contrast quantitative imaging make CMR even more available across all patient groups. In the meantime, post-processing can be used clinically to increase both precision and accuracy of CMR.

8 CONCLUSIONS

There are sex differences in several aspects of clinical, quantitative CMR imaging that affect diagnostic precision, and post-processing is a powerful tool to improve both precision and accuracy. Study-specific conclusions are:

- Blood correction increases precision in native myocardial T_1 values with 13% and eliminates sex differences in native myocardial T_1 values. Image-based correction of native myocardial T_1 is valid for clinical use. Blood correction may improve disease detection in the clinical evaluation of native myocardial T_1, as well as reduce the sample size needed for clinical research (Study I).
- Stationary tissue background correction increases precision in Qp/Qs in a clinical population, reduces the number of patients with a Qp/Qs outside the normal range and affects sex differences in Qp/Qs (Study II).
- MBV, myocardial perfusion and myocardial ECV are all higher in female healthy volunteers compared to males, and provide mechanistic insight into normal myocardial physiology (Study III).
- SynLGE can provide complementary confidence in the assessment of myocardial scarring in complement to convential LGE, and thereby increase diagnsotic accuracy and precision (Study IV).

9 ACKNOWLEDGEMENTS

All the wonderful colleagues at the **Department of Clinical Physiology,** who are too many to be named individually, at Karolinska University Hospital, for making my time spent there such a pleasure, no matter if it was regarding clinical work or research.

I want to acknowledge and thank all my friends, who have supported me through medical school, as well as during my PhD. Thank you for being such a light in my life, for all our dinners, game nights, and for keeping my spirits up no matter what. There are many, but I would especially like to mention **Jenny, Pontus and William Måhlberg, Jonas** and **Johanna Bergroth**, and **Ingrid Berggren** and **Peter Johansson**.

To my family, for being a constant source of warmth and inspiration, and for loving me regardless of my performance. **Mom, Dad, Jeanette and Jennie**, thank you for being my weird and loud supporter club, for all your encouraging words, and for always having my back.

Last, but absolutely not least, to the love of my life, my biggest supporter, my biggest critic, my past, future and present, the one who always feeds me, always makes me laugh and always makes me want to become a better person. **Fredrik Nickander**, you are more than my husband and more than my best friend, you are the reason for any success in my life, because of your unconditional love, your intellect and your untainted good-heartedness. I dedicate this work to you, because without you, there is no me. I love you.

10 REFERENCES

1.   Abraham, T.P., V.L. Dimaano, and H.Y. Liang, *Role of tissue Doppler and strain echocardiography in current clinical practice.* Circulation, 2007. **116**(22): p. 2597-609.

2.   Lam, W.C. and D.J. Pennell, *Imaging of the heart: historical perspective and recent advances.* Postgrad Med J, 2016. **92**(1084): p. 99-104.

3.   Cury, R.C., et al., *Comprehensive assessment of myocardial perfusion defects, regional wall motion, and left ventricular function by using 64-section multidetector CT.* Radiology, 2008. **248**(2): p. 466-75.

4.   Detrano, R., et al., *Coronary calcium as a predictor of coronary events in four racial or ethnic groups.* N Engl J Med, 2008. **358**(13): p. 1336-45.

5.   Litt, H.I., et al., *CT angiography for safe discharge of patients with possible acute coronary syndromes.* N Engl J Med, 2012. **366**(15): p. 1393-403.

6.   Priest, V.L., et al., *Cost-effectiveness of coronary computed tomography and cardiac stress imaging in the emergency department: a decision analytic model comparing diagnostic strategies for chest pain in patients at low risk of acute coronary syndromes.* JACC Cardiovasc Imaging, 2011. **4**(5): p. 549-56.

7.   Ghosh, N., et al., *Assessment of myocardial ischaemia and viability: role of positron emission tomography.* Eur Heart J, 2010. **31**(24): p. 2984-95.

8.   Di Carli, M., et al., *Relation among stenosis severity, myocardial blood flow, and flow reserve in patients with coronary artery disease.* Circulation, 1995. **91**(7): p. 1944-51.

9.   Uren, N.G., et al., *Relation between myocardial blood flow and the severity of coronary-artery stenosis.* N Engl J Med, 1994. **330**(25): p. 1782-8.

10.   Kim, R.J., et al., *The use of contrast-enhanced magnetic resonance imaging to identify reversible myocardial dysfunction.* N Engl J Med, 2000. **343**(20): p. 1445-53.

11.   Gupta, A., et al., *Myocardial infarction: optimization of inversion times at delayed contrast-enhanced MR imaging.* Radiology, 2004. **233**(3): p. 921-6.

12.   Hunold, P., et al., *Myocardial late enhancement in contrast-enhanced cardiac MRI: distinction between infarction scar and non-infarction-related disease.* AJR Am J Roentgenol, 2005. **184**(5): p. 1420-6.

13.   Mahrholdt, H., et al., *Delayed enhancement cardiovascular magnetic resonance assessment of non-ischaemic cardiomyopathies.* Eur Heart J, 2005. **26**(15): p. 1461-74.

14.   Friedrich, M.G., et al., *Contrast media-enhanced magnetic resonance imaging visualizes myocardial changes in the course of viral myocarditis.* Circulation, 1998. **97**(18): p. 1802-9.

15.   Ferreira, V.M., et al., *Non-contrast T1-mapping detects acute myocardial edema with high diagnostic accuracy: a comparison to T2-weighted cardiovascular magnetic resonance.* J Cardiovasc Magn Reson, 2012. **14**: p. 42.

16.	Schalla, S., et al., *Comparison of magnetic resonance real-time imaging of left ventricular function with conventional magnetic resonance imaging and echocardiography.* Am J Cardiol, 2001. **87**(1): p. 95-9.

17.	Kim, R.J., et al., *Relationship of MRI delayed contrast enhancement to irreversible injury, infarct age, and contractile function.* Circulation, 1999. **100**(19): p. 1992-2002.

18.	Lipton, M.J., et al., *Imaging of ischemic heart disease.* Eur Radiol, 2002. **12**(5): p. 1061-80.

19.	Mordini, F.E., et al., *Diagnostic accuracy of stress perfusion CMR in comparison with quantitative coronary angiography: fully quantitative, semiquantitative, and qualitative assessment.* JACC Cardiovasc Imaging, 2014. **7**(1): p. 14-22.

20.	McCommis, K.S., et al., *Quantification of myocardial blood volume during dipyridamole and doubtamine stress: a perfusion CMR study.* J Cardiovasc Magn Reson, 2007. **9**(5): p. 785-92.

21.	Arheden, H., et al., *Left-to-right cardiac shunts: comparison of measurements obtained with MR velocity mapping and with radionuclide angiography.* Radiology, 1999. **211**(2): p. 453-8.

22.	WHO. *The top 10 causes of death.* 2017 [cited 2018 February 8]; WHO Fact sheet]. Available from: http://www.who.int/mediacentre/factsheets/fs310/en/.

23.	CIHR. *Definitions of Sex and Gender.* 2015 [cited 2017 December 13]; Available from: http://www.cihr-irsc.gc.ca/e/47830.html.

24.	JCGM. *International Vocabulary of Metrology - Basic and General Concepts and Associated Terms (JCGM 200:2012).* 2012 [cited 2017 December 5]; VIM 3rd:[JCGM 200:2012 (JCGM 200:2008 with minor corrections)]. Available from: https://www.bipm.org/en/publications/guides/vim.html.

25.	Kellman, P. and M.S. Hansen, *T1-mapping in the heart: accuracy and precision.* J Cardiovasc Magn Reson, 2014. **16**: p. 2.

26.	Campbell, M.J., D. Machin, and S.J. Walter, *Medical Statistics: A Textbook for the Health Sciences.* 4 ed. 2007: John Wiley & Sons, Incorporated.

27.	Prince, M.R., et al., *Incidence of immediate gadolinium contrast media reactions.* AJR Am J Roentgenol, 2011. **196**(2): p. W138-43.

28.	Wertman, R., et al., *Risk of nephrogenic systemic fibrosis: evaluation of gadolinium chelate contrast agents at four American universities.* Radiology, 2008. **248**(3): p. 799-806.

29.	Kanda, T., et al., *High signal intensity in the dentate nucleus and globus pallidus on unenhanced T1-weighted MR images: relationship with increasing cumulative dose of a gadolinium-based contrast material.* Radiology, 2014. **270**(3): p. 834-41.

30.	Kanda, T., et al., *Gadolinium-based Contrast Agent Accumulates in the Brain Even in Subjects without Severe Renal Dysfunction: Evaluation of Autopsy Brain Specimens with Inductively Coupled Plasma Mass Spectroscopy.* Radiology, 2015. **276**(1): p. 228-32.

31.	Malayeri, A.A., et al., *National Institutes of Health Perspective on Reports of Gadolinium Deposition in the Brain.* J Am Coll Radiol, 2016. **13**(3): p. 237-41.

66

32.   Rabi, I.I., et al., *A New Method of Measuring Nuclear Magnetic Moment.* Physical Review, 1938. **53**(feb): p. 318-318.

33.   Bloch, F., *The Principle of Nuclear Induction.* Science, 1953. **118**(3068): p. 425-30.

34.   Larmor, J., *A dynamical theory of the electric and luminiferous medium. Part III. Relations with material media.* Proceedings of the Royal Society of London, 1897. **61**(369-377): p. 272-285.

35.   Carr, D.H., et al., *Intravenous chelated gadolinium as a contrast agent in NMR imaging of cerebral tumours.* Lancet, 1984. **1**(8375): p. 484-6.

36.   Mansfield, A.N.G.a.P.K.G.a.P., *Image formation in NMR by a selective irradiative process.* Journal of Physics C: Solid State Physics, 1974. **7**(24): p. L457.

37.   Lauterbur, P.C., *Image formation by induced local interactions. Examples employing nuclear magnetic resonance. 1973.* Clin Orthop Relat Res, 1989(244): p. 3-6.

38.   Ridgway, J.P., *Cardiovascular magnetic resonance physics for clinicians: part I.* J Cardiovasc Magn Reson, 2010. **12**: p. 71.

39.   Messroghli, D.R., et al., *Modified Look-Locker inversion recovery (MOLLI) for high-resolution T1 mapping of the heart.* Magn Reson Med, 2004. **52**(1): p. 141-6.

40.   Singer, J.R., *Blood Flow Rates by Nuclear Magnetic Resonance Measurements.* Science, 1959. **130**(3389): p. 1652-3.

41.   Moran, P.R., *A flow velocity zeugmatographic interlace for NMR imaging in humans.* Magn Reson Imaging, 1982. **1**(4): p. 197-203.

42.   van Dijk, P., *Direct cardiac NMR imaging of heart wall and blood flow velocity.* J Comput Assist Tomogr, 1984. **8**(3): p. 429-36.

43.   Bryant, D.J., et al., *Measurement of flow with NMR imaging using a gradient pulse and phase difference technique.* J Comput Assist Tomogr, 1984. **8**(4): p. 588-93.

44.   Nayler, G.L., D.N. Firmin, and D.B. Longmore, *Blood flow imaging by cine magnetic resonance.* J Comput Assist Tomogr, 1986. **10**(5): p. 715-22.

45.   Kellman, P., et al., *Myocardial perfusion cardiovascular magnetic resonance: optimized dual sequence and reconstruction for quantification.* J Cardiovasc Magn Reson, 2017. **19**(1): p. 43.

46.   Kellman, P., et al., *Extracellular volume fraction mapping in the myocardium, part 1: evaluation of an automated method.* J Cardiovasc Magn Reson, 2012. **14**: p. 63.

47.   Dall'Armellina, E., et al., *Cardiovascular magnetic resonance by non contrast T1-mapping allows assessment of severity of injury in acute myocardial infarction.* J Cardiovasc Magn Reson, 2012. **14**: p. 15.

48.   Ferreira, V.M., et al., *Native T1-mapping detects the location, extent and patterns of acute myocarditis without the need for gadolinium contrast agents.* J Cardiovasc Magn Reson, 2014. **16**: p. 36.

49.   Ferreira, V.M., et al., *T(1) mapping for the diagnosis of acute myocarditis using CMR: comparison to T2-weighted and late gadolinium enhanced imaging.* JACC Cardiovasc Imaging, 2013. **6**(10): p. 1048-58.

50.   Fontana, M., et al., *Native T1 mapping in transthyretin amyloidosis.* JACC Cardiovasc Imaging, 2014. **7**(2): p. 157-65.

51.   Feng, Y., et al., *In vivo comparison of myocardial T1 with T2 and T2* in thalassaemia major.* J Magn Reson Imaging, 2013. **38**(3): p. 588-93.

52.   Messroghli, D.R., et al., *Optimization and validation of a fully-integrated pulse sequence for modified look-locker inversion-recovery (MOLLI) T1 mapping of the heart.* J Magn Reson Imaging, 2007. **26**(4): p. 1081-6.

53.   Gai, N.D., et al., *Modified Look-Locker T1 evaluation using Bloch simulations: human and phantom validation.* Magn Reson Med, 2013. **69**(2): p. 329-36.

54.   Kellman, P., D.A. Herzka, and M.S. Hansen, *Adiabatic inversion pulses for myocardial T1 mapping.* Magn Reson Med, 2014. **71**(4): p. 1428-34.

55.   Kellman, P., et al., *Influence of Off-resonance in myocardial T1-mapping using SSFP based MOLLI method.* J Cardiovasc Magn Reson, 2013. **15**: p. 63.

56.   Kellman, P., A.E. Arai, and H. Xue, *T1 and extracellular volume mapping in the heart: estimation of error maps and the influence of noise on precision.* J Cardiovasc Magn Reson, 2013. **15**: p. 56.

57.   Piechnik, S.K., et al., *Shortened Modified Look-Locker Inversion recovery (ShMOLLI) for clinical myocardial T1-mapping at 1.5 and 3 T within a 9 heartbeat breathhold.* J Cardiovasc Magn Reson, 2010. **12**: p. 69.

58.   Chow, K., et al., *Saturation recovery single-shot acquisition (SASHA) for myocardial T(1) mapping.* Magn Reson Med, 2014. **71**(6): p. 2082-95.

59.   Xue, H., et al., *Phase-sensitive inversion recovery for myocardial T1 mapping with motion correction and parametric fitting.* Magn Reson Med, 2013. **69**(5): p. 1408-20.

60.   Piechnik, S.K., et al., *Normal variation of magnetic resonance T1 relaxation times in the human population at 1.5 T using ShMOLLI.* J Cardiovasc Magn Reson, 2013. **15**: p. 13.

61.   Hansen, M.S., et al., *Method for calculating confidence intervals for phase contrast flow measurements.* J Cardiovasc Magn Reson, 2014. **16**: p. 46.

62.   Hall, J.E., *Guyton and Hall textbook of medical physiology.* 12 ed. Textbook of Medical Physiology. 2011, Philadelphia: Saunders. 1168.

63.   Tohka, J., *Partial volume effect modeling for segmentation and tissue classification of brain magnetic resonance images: A review.* World J Radiol, 2014. **6**(11): p. 855-64.

64.   Lu, H., et al., *Determining the longitudinal relaxation time (T1) of blood at 3.0 Tesla.* Magn Reson Med, 2004. **52**(3): p. 679-82.

65.   Fullerton, G.D., J.L. Potter, and N.C. Dornbluth, *NMR relaxation of protons in tissues and other macromolecular water solutions.* Magn Reson Imaging, 1982. **1**(4): p. 209-26.

66.   Silvennoinen, M.J., M.I. Kettunen, and R.A. Kauppinen, *Effects of hematocrit and oxygen saturation level on blood spin-lattice relaxation.* Magn Reson Med, 2003. **49**(3): p. 568-71.

67.	Rosmini, S., *Hematocrit, Iron and Hdl-cholesterol Explain 90% of Variation in Native Blood T1*, in *Society for Cardiovascular Magnetic Resonance 19th Annual Scientific Sessions*. 2016: Hyatt Regency Century Plaza, Los Angeles, California, USA.

68.	Varela, M., et al., *A method for rapid in vivo measurement of blood T1.* NMR Biomed, 2011. **24**(1): p. 80-8.

69.	Tadamura, E., et al., *Effect of oxygen inhalation on relaxation times in various tissues.* J Magn Reson Imaging, 1997. **7**(1): p. 220-5.

70.	Wansapura, J., et al., *Cyclic variation of T1 in the myocardium at 3 T.* Magn Reson Imaging, 2006. **24**(7): p. 889-93.

71.	Reiter, U., et al., *Normal Diastolic and Systolic Myocardial T1 Values at 1.5-T MR Imaging: Correlations and Blood Normalization.* Radiology, 2013: p. 131225.

72.	Thygesen, K., et al., *Third universal definition of myocardial infarction.* Circulation, 2012. **126**(16): p. 2020-35.

73.	Caille, J.M., B. Lemanceau, and B. Bonnemain, *Gadolinium as a contrast agent for NMR.* AJNR Am J Neuroradiol, 1983. **4**(5): p. 1041-2.

74.	Arheden, H., et al., *Measurement of the distribution volume of gadopentetate dimeglumine at echo-planar MR imaging to quantify myocardial infarction: comparison with 99mTc-DTPA autoradiography in rats.* Radiology, 1999. **211**(3): p. 698-708.

75.	Kellman, P. and A.E. Arai, *Cardiac imaging techniques for physicians: late enhancement.* J Magn Reson Imaging, 2012. **36**(3): p. 529-42.

76.	Hsu, J.J. and I.J. Lowe, *Spin-lattice relaxation and a fast T1-map acquisition method in MRI with transient-state magnetization.* J Magn Reson, 2004. **169**(2): p. 270-8.

77.	Kellman, P., et al., *Phase-sensitive inversion recovery for detecting myocardial infarction using gadolinium-delayed hyperenhancement.* Magn Reson Med, 2002. **47**(2): p. 372-83.

78.	Hsu, J.J. and G.H. Glover, *Rapid MRI method for mapping the longitudinal relaxation time.* J Magn Reson, 2006. **181**(1): p. 98-106.

79.	Karamitsos, T.D., et al., *Noncontrast T1 mapping for the diagnosis of cardiac amyloidosis.* JACC Cardiovasc Imaging, 2013. **6**(4): p. 488-97.

80.	Ugander, M., et al., *Extracellular volume imaging by magnetic resonance imaging provides insights into overt and sub-clinical myocardial pathology.* Eur Heart J, 2012. **33**(10): p. 1268-78.

81.	Miller, C.A., et al., *Comprehensive validation of cardiovascular magnetic resonance techniques for the assessment of myocardial extracellular volume.* Circ Cardiovasc Imaging, 2013. **6**(3): p. 373-83.

82.	Socialstyrelsen, *Hjärtinfarkter 1988-2012*. 2013, SVERIGES OFFICIELLA STATISTIK (SOS).

83.	Bucholz, E.M. and H.M. Krumholz, *Women in clinical research: what we need for progress*, in *Circ Cardiovasc Qual Outcomes*. 2015: United States. p. S1-3.

84.	Carlsson, M., et al., *Cardiac output and cardiac index measured with cardiovascular magnetic resonance in healthy subjects, elite athletes and patients with congestive heart failure.* J Cardiovasc Magn Reson, 2012. **14**: p. 51.

85.	Umetani, K., et al., *Twenty-four hour time domain heart rate variability and heart rate: relations to age and gender over nine decades.* J Am Coll Cardiol, 1998. **31**(3): p. 593-601.

86.	Maceira, A.M., et al., *Normalized left ventricular systolic and diastolic function by steady state free precession cardiovascular magnetic resonance.* J Cardiovasc Magn Reson, 2006. **8**(3): p. 417-26.

87.	Kawel-Boehm, N., et al., *Normal values for cardiovascular magnetic resonance in adults and children.* J Cardiovasc Magn Reson, 2015. **17**: p. 29.

88.	Davies, M.J., *Anatomic features in victims of sudden coronary death. Coronary artery pathology.* Circulation, 1992. **85**(1 Suppl): p. I19-24.

89.	DeWood, M.A., et al., *Prevalence of total coronary occlusion during the early hours of transmural myocardial infarction.* N Engl J Med, 1980. **303**(16): p. 897-902.

90.	Khan, N.A., et al., *Sex differences in prodromal symptoms in acute coronary syndrome in patients aged 55 years or younger.* Heart, 2017. **103**(11): p. 863-869.

91.	Stone, G.W., et al., *A prospective natural-history study of coronary atherosclerosis.* N Engl J Med, 2011. **364**(3): p. 226-35.

92.	Mason, R.E., et al., *Multiple-lead exercise electrocardiography. Experience in 107 normal subjects and 67 patients with angina pectoris, and comparison with coronary cinearteriography in 84 patients.* Circulation, 1967. **36**(4): p. 517-25.

93.	al-Khalili, F., et al., *Intracoronary ultrasound measurements in women with myocardial infarction without significant coronary lesions.* Coron Artery Dis, 2000. **11**(8): p. 579-84.

94.	Farb, A., et al., *Coronary plaque erosion without rupture into a lipid core. A frequent cause of coronary thrombosis in sudden coronary death.* Circulation, 1996. **93**(7): p. 1354-63.

95.	van der Wal, A.C., et al., *Site of intimal rupture or erosion of thrombosed coronary atherosclerotic plaques is characterized by an inflammatory process irrespective of the dominant plaque morphology.* Circulation, 1994. **89**(1): p. 36-44.

96.	Libby, P. and G. Pasterkamp, *Requiem for the 'vulnerable plaque'.* Eur Heart J, 2015. **36**(43): p. 2984-7.

97.	Ibanez, B., et al., *2017 ESC Guidelines for the management of acute myocardial infarction in patients presenting with ST-segment elevation: The Task Force for the management of acute myocardial infarction in patients presenting with ST-segment elevation of the European Society of Cardiology (ESC).* Eur Heart J, 2017.

98.	Roffi, M., et al., *2015 ESC Guidelines for the management of acute coronary syndromes in patients presenting without persistent ST-segment elevation: Task Force for the Management of Acute Coronary Syndromes in Patients Presenting without Persistent ST-Segment Elevation of the European Society of Cardiology (ESC).* Eur Heart J, 2016. **37**(3): p. 267-315.

99.	Apple, F.S. and A.S. Jaffe, *Men are different than women: it's true for cardiac troponin too.* Clin Biochem, 2014. **47**(10-11): p. 867-8.

100.	Eggers, K.M., et al., *Cardiac troponin I levels in patients with non-ST-elevation acute coronary syndrome-the importance of gender.* Am Heart J, 2014. **168**(3): p. 317-324.e1.

101.   Schenck-Gustafsson, K. and N. Johnston-Holmström, *Kvinnohjärtan - hjärt-och kärlsjukdomar hos kvinnor*. 2017, Uppsala: Studentlitteratur. 277.

102.   Bairey Merz, C.N., et al., *Ischemia and No Obstructive Coronary Artery Disease (INOCA): Developing Evidence-Based Therapies and Research Agenda for the Next Decade.* Circulation, 2017. **135**(11): p. 1075-1092.

103.   Jespersen, L., et al., *Stable angina pectoris with no obstructive coronary artery disease is associated with increased risks of major adverse cardiovascular events.* Eur Heart J, 2012. **33**(6): p. 734-44.

104.   Berry, C., *Stable Coronary Syndromes: The Case for Consolidating the Nomenclature of Stable Ischemic Heart Disease.* Circulation, 2017. **136**(5): p. 437-439.

105.   Daly, C., et al., *Gender differences in the management and clinical outcome of stable angina.* Circulation, 2006. **113**(4): p. 490-8.

106.   Montalescot, G., et al., *2013 ESC guidelines on the management of stable coronary artery disease: the Task Force on the management of stable coronary artery disease of the European Society of Cardiology.* Eur Heart J, 2013. **34**(38): p. 2949-3003.

107.   Knol, R.J.J., et al., *Exercise Electrocardiogram Neither Predicts Nor Excludes Coronary Artery Disease in Women with Low to Intermediate Risk.* J Womens Health (Larchmt), 2018.

108.   NICE. *Chest pain of recent onset: assessment and diagnosis*. 2016 [cited 2018 February 12]; Clinical guideline [CG95]]. Available from: https://www.nice.org.uk/Guidance/CG95.

109.   Williams, M.C., et al., *Symptoms and quality of life in patients with suspected angina undergoing CT coronary angiography: a randomised controlled trial.* Heart, 2017.

110.   Feher, A. and A.J. Sinusas, *Quantitative Assessment of Coronary Microvascular Function: Dynamic Single-Photon Emission Computed Tomography, Positron Emission Tomography, Ultrasound, Computed Tomography, and Magnetic Resonance Imaging.* Circ Cardiovasc Imaging, 2017. **10**(8).

111.   Maher, V.M., *Coronary atherosclerosis stabilization: an achievable goal.* Atherosclerosis, 1995. **118 Suppl**: p. S91-101.

112.   Picano, E., S. Molinaro, and E. Pasanisi, *The diagnostic accuracy of pharmacological stress echocardiography for the assessment of coronary artery disease: a meta-analysis.* Cardiovasc Ultrasound, 2008. **6**: p. 30.

113.   Schwitter, J., et al., *Assessment of myocardial perfusion in coronary artery disease by magnetic resonance: a comparison with positron emission tomography and coronary angiography.* Circulation, 2001. **103**(18): p. 2230-5.

114.   Schwitter, J., et al., *Magnetic resonance-based assessment of global coronary flow and flow reserve and its relation to left ventricular functional parameters: a comparison with positron emission tomography.* Circulation, 2000. **101**(23): p. 2696-702.

115.   Mahmod, M., et al., *Adenosine stress native T1 mapping in severe aortic stenosis: evidence for a role of the intravascular compartment on myocardial T1 values.* J Cardiovasc Magn Reson, 2014. **16**: p. 92.

116.   Manisty, C., et al., *Splenic Switch-off: A Tool to Assess Stress Adequacy in Adenosine Perfusion Cardiac MR Imaging.* Radiology, 2015. **276**(3): p. 732-40.

117.   Heiberg, E., et al., *Design and validation of Segment--freely available software for cardiovascular image analysis.* BMC Med Imaging, 2010. **10**: p. 1.

118.   Schelbert, E.B., et al., *Myocardial extravascular extracellular volume fraction measurement by gadolinium cardiovascular magnetic resonance in humans: slow infusion versus bolus.* J Cardiovasc Magn Reson, 2011. **13**: p. 16.

119.   Reiter, U., et al., *Native myocardial T1 mapping in pulmonary hypertension: correlations with cardiac function and hemodynamics.* Eur Radiol, 2017. **27**(1): p. 157-166.

120.   O'Mahony, C. and P. Elliott, *Anderson-Fabry disease and the heart.* Prog Cardiovasc Dis, 2010. **52**(4): p. 326-35.

121.   Weingartner, S., et al., *Combined saturation/inversion recovery sequences for improved evaluation of scar and diffuse fibrosis in patients with arrhythmia or heart rate variability.* Magn Reson Med, 2014. **71**(3): p. 1024-34.

122.   Roujol, S., et al., *Accuracy, precision, and reproducibility of four T1 mapping sequences: a head-to-head comparison of MOLLI, ShMOLLI, SASHA, and SAPPHIRE.* Radiology, 2014. **272**(3): p. 683-9.

123.   Chow, K., et al., *Robust free-breathing SASHA T1 mapping with high-contrast image registration.* J Cardiovasc Magn Reson, 2016. **18**(1): p. 47.

124.   Weingartner, S., et al., *Myocardial T1-mapping at 3T using saturation-recovery: reference values, precision and comparison with MOLLI.* J Cardiovasc Magn Reson, 2016. **18**(1): p. 84.

125.   Wong, T.C., et al., *Association between extracellular matrix expansion quantified by cardiovascular magnetic resonance and short-term mortality.* Circulation, 2012. **126**(10): p. 1206-16.

126.   Meierhofer, C., et al., *Baseline correction does not improve flow quantification in phase-contrast velocity measurement for routine clinical practice.* Clin Imaging, 2015. **39**(3): p. 427-31.

127.   Baritussio, A., A. Scatteia, and C. Bucciarelli-Ducci, *Role of cardiovascular magnetic resonance in acute and chronic ischemic heart disease.* Int J Cardiovasc Imaging, 2018. **34**(1): p. 67-80.

128.   Niccoli, G., G. Scalone, and F. Crea, *Acute myocardial infarction with no obstructive coronary atherosclerosis: mechanisms and management.* Eur Heart J, 2015. **36**(8): p. 475-81.

129.   Gehrie, E.R., et al., *Characterization and outcomes of women and men with non-ST-segment elevation myocardial infarction and nonobstructive coronary artery disease: results from the Can Rapid Risk Stratification of Unstable Angina Patients Suppress Adverse Outcomes with Early Implementation of the ACC/AHA Guidelines (CRUSADE) quality improvement initiative.* Am Heart J, 2009. **158**(4): p. 688-94.

130.   Dastidar, A.G., et al., *The Role of Cardiac MRI in Patients with Troponin-Positive Chest Pain and Unobstructed Coronary Arteries.* Curr Cardiovasc Imaging Rep, 2015. **8**(8): p. 28.

131.   Pathik, B., et al., *Troponin-positive chest pain with unobstructed coronary arteries: incremental diagnostic value of cardiovascular magnetic resonance imaging.* Eur Heart J Cardiovasc Imaging, 2016. **17**(10): p. 1146-52.

132.   Dastidar, A.G., et al., *Myocardial Infarction With Nonobstructed Coronary Arteries: Impact of CMR Early After Presentation.* JACC Cardiovasc Imaging, 2017. **10**(10 Pt A): p. 1204-1206.

133.   Bucciarelli-Ducci, C., et al., *CMR Guidance for Recanalization of Coronary Chronic Total Occlusion.* JACC Cardiovasc Imaging, 2016. **9**(5): p. 547-56.

134.   Windecker, S., et al., *2014 ESC/EACTS Guidelines on myocardial revascularization: The Task Force on Myocardial Revascularization of the European Society of Cardiology (ESC) and the European Association for Cardio-Thoracic Surgery (EACTS)Developed with the special contribution of the European Association of Percutaneous Cardiovascular Interventions (EAPCI).* Eur Heart J, 2014. **35**(37): p. 2541-619.

135.   Vaccarino, V., et al., *Sex differences in mortality after myocardial infarction: evidence for a sex-age interaction.* Arch Intern Med, 1998. **158**(18): p. 2054-62.

136.   Champney, K.P., et al., *The joint contribution of sex, age and type of myocardial infarction on hospital mortality following acute myocardial infarction.* Heart, 2009. **95**(11): p. 895-9.

137.   Izadnegahdar, M., et al., *Do younger women fare worse? Sex differences in acute myocardial infarction hospitalization and early mortality rates over ten years.* J Womens Health (Larchmt), 2014. **23**(1): p. 10-7.

138.   Egiziano, G., et al., *Sex differences in young patients with acute myocardial infarction.* Diabet Med, 2013. **30**(3): p. e108-14.

139.   Nazzal, C. and F.T. Alonso, *Younger women have a higher risk of in-hospital mortality due to acute myocardial infarction in Chile.* Rev Esp Cardiol (Engl Ed), 2013. **66**(2): p. 104-9.

140.   Gupta, A., et al., *Trends in acute myocardial infarction in young patients and differences by sex and race, 2001 to 2010.* J Am Coll Cardiol, 2014. **64**(4): p. 337-45.

141.   Zhang, Z., et al., *Age-specific gender differences in in-hospital mortality by type of acute myocardial infarction.* Am J Cardiol, 2012. **109**(8): p. 1097-103.

142.   Khan, N.A., et al., *Sex differences in acute coronary syndrome symptom presentation in young patients.* JAMA Intern Med, 2013. **173**(20): p. 1863-71.

143.   Pelletier, R., et al., *Depression and disease severity in patients with premature acute coronary syndrome.* Am J Med, 2014. **127**(1): p. 87-93.e1-2.

144.   Lee, T.M., T.F. Chou, and C.H. Tsai, *Effect of estrogen on coronary vasoconstriction in patients undergoing coronary angioplasty.* Int J Cardiol, 2005. **101**(3): p. 465-72.

145.   Camici, P.G. and F. Crea, *Coronary microvascular dysfunction.* N Engl J Med, 2007. **356**(8): p. 830-40.

146.   Gould, K.L., et al., *Anatomic versus physiologic assessment of coronary artery disease. Role of coronary flow reserve, fractional flow reserve, and positron emission tomography imaging in revascularization decision-making.* J Am Coll Cardiol, 2013. **62**(18): p. 1639-1653.

147.   Stuijfzand, W.J., et al., *Relative flow reserve derived from quantitative perfusion imaging may not outperform stress myocardial blood flow for identification of hemodynamically significant coronary artery disease.* Circ Cardiovasc Imaging, 2015. **8**(1).

148.   Danad, I., et al., *Quantitative assessment of myocardial perfusion in the detection of significant coronary artery disease: cutoff values and diagnostic accuracy of quantitative [(15)O]H2O PET imaging.* J Am Coll Cardiol, 2014. **64**(14): p. 1464-75.

149.   Murthy, V.L., et al., *Effects of sex on coronary microvascular dysfunction and cardiac outcomes.* Circulation, 2014. **129**(24): p. 2518-27.

150.   De Bruyne, B., et al., *Fractional flow reserve-guided PCI versus medical therapy in stable coronary disease.* N Engl J Med, 2012. **367**(11): p. 991-1001.

151.   Pijls, N.H., et al., *Fractional flow reserve versus angiography for guiding percutaneous coronary intervention in patients with multivessel coronary artery disease: 2-year follow-up of the FAME (Fractional Flow Reserve Versus Angiography for Multivessel Evaluation) study.* J Am Coll Cardiol, 2010. **56**(3): p. 177-84.

152.   Tonino, P.A., et al., *Fractional flow reserve versus angiography for guiding percutaneous coronary intervention.* N Engl J Med, 2009. **360**(3): p. 213-24.

153.   Gould, K.L. and N.P. Johnson, *Physiologic stenosis severity, binary thinking, revascularization, and "hidden reality".* Circ Cardiovasc Imaging, 2015. **8**(1).

154.   van Horssen, P., et al., *Perfusion territories subtended by penetrating coronary arteries increase in size and decrease in number toward the subendocardium.* Am J Physiol Heart Circ Physiol, 2014. **306**(4): p. H496-504.

155.   Hedstrom, E., et al., *Infarct evolution in man studied in patients with first-time coronary occlusion in comparison to different species - implications for assessment of myocardial salvage.* J Cardiovasc Magn Reson, 2009. **11**: p. 38.

156.   Johnson, N.P. and K.L. Gould, *Integrating noninvasive absolute flow, coronary flow reserve, and ischemic thresholds into a comprehensive map of physiological severity.* JACC Cardiovasc Imaging, 2012. **5**(4): p. 430-40.

157.   Gupta, A., et al., *Integrated Noninvasive Physiological Assessment of Coronary Circulatory Function and Impact on Cardiovascular Mortality in Patients With Stable Coronary Artery Disease.* Circulation, 2017. **136**(24): p. 2325-2336.

158.   Johnson, N.P., et al., *Prognostic value of fractional flow reserve: linking physiologic severity to clinical outcomes.* J Am Coll Cardiol, 2014. **64**(16): p. 1641-54.

159.   Toth, G., et al., *Evolving concepts of angiogram: fractional flow reserve discordances in 4000 coronary stenoses.* Eur Heart J, 2014. **35**(40): p. 2831-8.

160.   Liu, A., et al., *Adenosine Stress and Rest T1 Mapping Can Differentiate Between Ischemic, Infarcted, Remote, and Normal Myocardium Without the Need for Gadolinium Contrast Agents.* JACC Cardiovasc Imaging, 2016. **9**(1): p. 27-36.

161.   Liu, A., et al., *Gadolinium-Free Cardiac MR Stress T1-Mapping to Distinguish Epicardial From Microvascular Coronary Disease.* J Am Coll Cardiol, 2018. **71**(9): p. 957-968.

162.   Engblom, H., et al., *Fully quantitative cardiovascular magnetic resonance myocardial perfusion ready for clinical use: a comparison between cardiovascular magnetic resonance imaging and positron emission tomography.* J Cardiovasc Magn Reson, 2017. **19**(1): p. 78.

163.   Wei, K., et al., *Quantification of myocardial blood flow with ultrasound-induced destruction of microbubbles administered as a constant venous infusion.* Circulation, 1998. **97**(5): p. 473-83.

164.   Vogel, R., et al., *The quantification of absolute myocardial perfusion in humans by contrast echocardiography: algorithm and validation.* J Am Coll Cardiol, 2005. **45**(5): p. 754-62.

165.   Varga-Szemes, A., et al., *Myocardial Late Gadolinium Enhancement: Accuracy of T1 Mapping-based Synthetic Inversion-Recovery Imaging.* Radiology, 2016. **278**(2): p. 374-82.

166.   Bulluck, H., et al., *Quantification of both the area-at-risk and acute myocardial infarct size in ST-segment elevation myocardial infarction using T1-mapping.* J Cardiovasc Magn Reson, 2017. **19**(1): p. 57.